View metadata, citation and similar papers at core.ac.uk

brought to you by CORE

provided by College of William & Mary: W&M Publish

W&M ScholarWorks

VIMS Articles

2002

Examination of diffusion versus advection dominated sediment suspension on the inner shelf under storm and swell conditions, Duck, North Carolina

Guan-hong Lee
Virginia Institute of Marine Science

Carl T. Friedrichs
Virginia Institute of Marine Science, carl.friedrichs@vims.edu

Chris E. Vincent
University of East Anglia

Follow this and additional works at: https://scholarworks.wm.edu/vimsarticles

 Part of the Marine Biology Commons

Recommended Citation

Lee, Guan-hong; Friedrichs, Carl T.; and Vincent, Chris E., "Examination of diffusion versus advection dominated sediment suspension on the inner shelf under storm and swell conditions, Duck, North Carolina" (2002). *VIMS Articles*. 282.
https://scholarworks.wm.edu/vimsarticles/282

This Article is brought to you for free and open access by W&M ScholarWorks. It has been accepted for inclusion in VIMS Articles by an authorized administrator of W&M ScholarWorks. For more information, please contact scholarworks@wm.edu.

Examination of diffusion versus advection dominated sediment suspension on the inner shelf under storm and swell conditions, Duck, North Carolina

Guan-hong Lee[1] and Carl T. Friedrichs

Virginia Institute of Marine Science, School of Marine Science, College of William and Mary, Gloucester Point, Virginia, USA

Chris E. Vincent

School of Environmental Science, University of East Anglia, Norwich, England, UK

Received 10 April 2001; revised 17 October 2001; accepted 6 November 2001; published 30 July 2002.

[1] A benthic boundary layer tripod supporting six current meters and three profiling acoustic backscatter sensors (ABS) documented storm and swell conditions during the fall of 1996 at a depth of 13 m on the inner shelf off Duck, North Carolina. Sediment concentration was higher in the wave boundary layer (WBL) during storm conditions but higher ~40 cm above the bed (cm ab) during swell conditions. To test the applicability of a diffusive balance during storm versus swell, ABS data were used to invert the vertical diffusion equation and solve for eddy diffusivity from 1 to 50 cm ab. During the storm period, diffusivity derived from the ABS up to ~40 cm ab agreed well with viscosity derived above the WBL from observed current profiles and from the Grant-Madsen-Glenn (GMG) model. During the swell period, diffusivity derived from the ABS up to ~40 cm ab did not agree with observed mean current shear above this level nor with the GMG model. Diffusivity did agree with viscosity derived from shear stress due to waves within the WBL extrapolated to a height greater than the modeled WBL. We speculate that during swell conditions, shedding vortices enhanced mass and momentum exchange, extending the eddy viscosity associated with waves above the predicted WBL; during storm conditions, strong currents prevented vortices from penetrating beyond the predicted WBL. Rouse diffusion models with two- and three-layered eddy diffusivity and combined diffusion-advection models with one and three-layer were applied to the observational data set. During the storm the two- and three-layered Rouse models including multiple grain sizes and bed armoring reproduced the observed concentration well. During swell (weak current conditions) all the models considered underpredicted the observed concentration if applied with a standard WBL thickness. To correct this, enhanced vertical exchange was represented by a thickened WBL whenever mean currents were weak relative to the estimated jet velocity associated with wave-induced vortex shedding. The two-layer Rouse model then reproduced the concentrations observed during swell remarkably well. This implies that mean sediment suspension dominated by wave-induced advection may still be approximated by a diffusion-like process under some circumstances. *INDEX TERMS:* 4211 Oceanography: General: Benthic boundary layers; 4558 Oceanography: Physical: Sediment transport; 4568 Oceanography: Physical: Turbulence, diffusion, and mixing processes; 4546 Oceanography: Physical: Nearshore processes; *KEYWORDS:* sediment, suspension, diffusion, advection, turbulence, Duck, North Carolina

1. Introduction

[2] In the shelf environment, sediment resuspension and transport occur owing to the combined action of waves and currents. An approach widely used to predict sediment transport rates for relatively fine sediment on shelves in the absence of pronounced wave asymmetry has been to determine the time-averaged, vertical profile of horizontal velocity u and the time-averaged profile of sediment concentration C and then to calculate the profile of suspended sediment flux, uC, with the assumption that sediments are transported horizontally with the mean velocity. As sediment becomes coarser and waves become more asymmetric, wave-induced transport must also be considered. Many models used in shelf sediment transport applications predict

[1]Now at Institute of Theoretical Geophysics, University of Cambridge, Cambridge, England.

Copyright 2002 by the American Geophysical Union.
0148-0227/02/2001JC000918

the time-averaged profile of sediment concentration for combined waves and currents by solving the steady state diffusion equation [e.g., *Smith*, 1977; *Sleath*, 1984; *Glenn and Grant*, 1987].

[3] The rate of change of the suspended sediment concentration at a certain elevation above the bed, z, is given by the equation of sediment volume conservation, assuming that the horizontal gradients are negligible relative to the vertical gradients

$$\partial C(t)/\partial t = w_s \partial C(t)/\partial z - \partial q_z/\partial z, \tag{1}$$

where $C(t)$ is the instantaneous concentration of the suspended sediment, q_z is the upward flux of the sediment, and w_s is sediment fall velocity. In the sediment diffusion model, q_z is generally described in terms of gradient diffusion

$$q_z = -\epsilon_s \partial C/\partial z. \tag{2}$$

The diffusive flux is proportional to the concentration gradient $\partial C/\partial z$ and to the sediment diffusivity ϵ_s. Integration of equation (1), after substituting equation (2) into equation (1) and taking a time average, results in the steady state diffusion equation:

$$w_s C + \epsilon_s \partial C/\partial z = 0, \tag{3}$$

where C now indicates the time-averaged concentration. Equation (3) simply states that the mechanism for time-averaged sediment suspension is a diffusive process such that upward sediment flux by turbulent diffusion is balanced by downward flux due to gravitational settling.

[4] To obtain an expression for ϵ_s, one common assumption is that

$$\epsilon_s = \epsilon_m = \kappa u_{*_{cw}} z \qquad z \le \delta_w, \tag{4a}$$

$$\epsilon_s = \epsilon_m = \kappa u_{*_c} z \qquad z \ge \delta_w, \tag{4b}$$

where ϵ_m is eddy viscosity, κ is von Karman's constant ($\sim$0.4), u_{*cw} is shear velocity due to the combined effect of waves and current inside the wave boundary layer (WBL) of thickness $\delta_w = 2\kappa u_{*cw}/\omega$, ω is wave radian frequency, and u_{*c} is shear velocity due to currents outside δ_w [*Grant and Madsen*, 1986; *Glenn and Grant*, 1987]. Using acoustic backscatter sensor (ABS) data to invert (3), *Vincent and Downing* [1994] reported that eddy diffusivity profiles, under combined waves and currents, increased linearly from the bed level to $\sim$20 cm above the bed and decreased above that level. Other authors have also found linearly increasing eddy diffusivity near the bed to be scaled by the characteristic shear velocity [*Sheng and Hay*, 1995; *Vincent and Osborne*, 1995]. The vertical length scale of the coherent diffusivity profile and its behavior above the linear region are subject to further research and first-hand discussion on the subject can be found in the work of *Sheng and Hay* [1995]. Thus it is reasonable to take a linearly increasing eddy viscosity model at least in the near-bottom region. Integration of equation (3) using equation (4) yields the Rouse equation. This approach has been widely used in the shelf environment [e.g., *Glenn and Grant*, 1987; *Vincent and Green*, 1990; *Li et al.*, 1997; *Lynch et al.*, 1997] and the vertical distribution of suspended sediment predicted by the Rouse equation is reported to agree also with measurements in unidirectional stream flow [e.g., *Vanoni*, 1975] and over a plane bed under waves in laboratory flumes [e.g., *Ribberink and Al-Salem*, 1994].

[5] The diffusion-settling balance can be a good approximation close to the bed when the turbulent diffusion process is dominant, for example, during a storm event. However, this balance may not hold when mechanisms other than diffusion are at work. When sharp-crested ripples are present under regular waves, laboratory results indicate that the dominant process of sediment suspension is no longer turbulent diffusion but rather vertical advection associated with the cyclic development and convection of large vortices [e.g., *Sleath*, 1982; *Ribberink and Al-Salem*, 1994]. The vertical distribution of suspended sediment over ripples for laboratory data has been described by equation (3) with constant eddy diffusivity, resulting in exponential profiles. In this context, eddy diffusivity represents the efficiency with which vortices eject sediment up into the water column. Both laboratory measurements [e.g., *Sleath*, 1982; *Dick and Sleath*, 1991; *Van Rijn et al.*, 1993; *Ribberink and Al-Salem*, 1994] and field measurements [e.g., *Nielsen*, 1984; *Wai et al.*, 1991; *Vincent and Osborne*, 1995] of sediment concentration have been fitted to exponential profiles when wave-induced bedforms were present and sediment advection by shedding vortices was observed (in the laboratory) or inferred (in the field).

[6] To address vertical advection by vortices over bedforms, *Nielsen* [1992] proposed a wave-averaged advection model of the form

$$w_s C - PF(z) = 0, \tag{5}$$

where $F(z)$ is the probability function that a given particle can reach a certain level, z, and $P = w_s C_r$ is the pickup rate, where C_r is the reference concentration. Empirical results suggest a probability function of the form

$$F(z) = \left[1 + 11z(k_b' A_b)^{-1/2}\right]^{-2}, \tag{6}$$

where k_b' is the bed roughness and A_b is the near-bottom orbital excursion. Nielsen further argued that in the presence of both advection and diffusion, the vertical distribution of suspended sediment can be described by a combined model that incorporates both effects. The steady state combined diffusion and advection equation of Nielsen is given by

$$w_s C + \epsilon_s dC/dz - PF(z) = 0. \tag{7}$$

Nielsen assumes the eddy diffusivity is constant with height such that

$$\epsilon_s = 0.016\omega k_b' A_b. \tag{8}$$

[7] The combined advection and diffusion approach was tested by *Lee and Hanes* [1996] using ABS data collected

under combined waves and currents. However, Lee and Hanes used a linearly increasing three-layered eddy viscosity model of *Madsen and Wikramanayake* [1991] instead of constant eddy viscosity and examined three suspension models: pure diffusion, pure advection, and combined diffusion and advection. The model of Madsen and Wikramanayake is similar to equation (4), but with an intermediate constant ϵ_s layer inserted to keep ε_s continuous. Lee and Hanes showed that the pure diffusion and the combined diffusion and advection models with graded sands predicted the observed concentration well under high energy conditions. Under low-energy conditions (with small ripples present) the combined diffusion and advection model performed best among the models, but it still underpredicted the steep concentration profiles observed above 10 cm above the bed (cm ab hereafter) (see Figure 6 of *Lee and Hanes* [1996]).

[8] Previous studies reviewed here indicate that under high-energy conditions turbulent diffusion is probably the dominant process for vertical mixing. Under high energy the assumption of equation (4), perhaps slightly modified following *Madsen and Wikramanayake* [1991], appears to be reasonable and the diffusion model of equation (3) adequately describes the vertical distribution of suspended sediments. Under low-energy conditions when bedforms are present and vortex shedding is the dominant vertical mixing process, the assumption of equation (4) is expected to fail and the vertical distribution of suspended sediments is not expected to be well represented by equation (3). The advection model or the combined diffusion and advection model is expected to do better.

[9] To determine which mechanism for suspending sediments is dominant and which model for the vertical distribution of suspended sediment is appropriate, it is essential to further examine the assumption of equation (4). Thus this paper investigates the relationship between eddy viscosity and eddy diffusivity during storm and swell conditions (section 3) by using flow and concentration data observed on the inner shelf off Duck, North Carolina (section 2). Then, the predictive ability of Rouse-type diffusion models are examined in conjunction with the assumption of equation (4) (section 4). This is followed by determining under what conditions the assumptions of equations (3) and (4) are valid (section 5). Recently, the relative strength of waves and currents has been reported to be important in influencing the types of bedforms present and the resulting pattern of sediment suspension [e.g., *Van Rijn et al.*, 1993; *Amos et al.*, 1998]. However, the effect of the relative strength of waves and currents on the detailed profile of eddy diffusivity and sediment concentration has not been well quantified. Thus we attempt to quantify this by parameterizing the relative strength of waves and currents. Finally, we compare the ability of combined advection and diffusion models and introduce a Rouse model with a thickened WBL to better reproduce observed sediment concentration profiles (sections 6 and 7).

2. Field Experiment and Environmental Conditions

2.1. Study Site

[10] The Virginia Institute of Marine Science deployed an instrumented benthic boundary layer tripod at depth of 13 m on the inner shelf off Duck, North Carolina (Figure 1), during 26 September to 22 October 1996. This area has relatively straight, simple offshore bathymetry. The inner shelf profile is concave upward over the region extending from the surf zone to about the 15-m isobath. Bottom sediments (<10 cm) are moderately well sorted, ranging from medium to fine sand. Silts and clays comprise less than 10% of the surficial sediment. Median sediment size of diver-collected samples was 120 μm.

[11] Tides at the Field Research Facility are semidiurnal with a mean range of ~1 m (spring tide range ≈ 1.2 m). Average annual significant wave height is 1.0 m (1980–1991) with a standard deviation of ±0.6 m, having a mean peak spectral period of 8.3 ± 2.6 s [*Leffler et al.*, 1993]. Wave energy is usually higher during the winter months and lower during the spring and summer. Longshore current speed and direction display seasonal trends. Frequent, short-term reversals of the current are common, but it is generally directed to the north in the summer months and southward during the winter. Storm occurrences are dominated by frequent extratropical northeasters during the fall, winter, and early spring months and occasionally by tropical storms and hurricanes during the summer and fall season. *Birkemeier et al.* [1985] provide a more detailed description of the site.

2.2. Pod Instrumentation and Data Analysis

[12] Instrumentation consisted of five electromagnetic current meters (EMCMs), at initial heights of 8, 38, 68, 98, and 125 cm above the bottom (ab), one pressure sensor (195 cm ab), three transceiver acoustic backscatter sensors (ABSs: all 88 cm ab) and one acoustic Doppler velocimeter (ADV: 19 cm ab). A sediment trap was mounted on a leg of the pod 100 cm ab. Instrument configuration is shown in Figure 2. The EMCMs and pressure sensor recorded data at 1 Hz for burst durations of 34 min at 2-hour intervals, while the ABS and ADV recorded data at 5 Hz for about 12 min at 2-hour intervals. The data were recorded in self-contained data loggers. The tripod was also equipped with optical backscatter sensors (OBSs), which unfortunately fouled badly, and thus OBS data were not used in this study.

[13] Estimation of wave characteristics utilized a current meter initially located 98 cm ab. Wave components were determined by removing the mean velocity components from each burst. Wave directions were defined as the direction of maximum variance for each burst [*Madsen et al.*, 1993]. Within a burst variance of each bin (1°) was estimated by

$$\sigma_\theta = \sum_{\theta}^{\theta+1} \left(\tilde{u}^2 + \tilde{v}^2\right), \tag{9}$$

where $\tilde{u}$ and $\tilde{v}$ are the oscillatory components of u and v, respectively. Each bin was then averaged using an 11° low pass filter. The root mean squared (rms) wave orbital velocity for each burst was calculated from $u_b = \sqrt{2}\,\boldsymbol{\sigma}_u$, where $\sigma_u{}^2$ is the total variance of the oscillatory flow $\left(\boldsymbol{\sigma}_u^2 = \sum_{\theta=1}^{360} \boldsymbol{\sigma}_\theta\right)$. The wave orbital velocity was rotated to the dominant wave direction, and the dominant wave period was estimated by using the zero up-crossing method.

[14] Three ABSs, whose acoustic frequencies are 1 (F1), 2 (F2), and 5 (F3) MHz and pulse lengths are ~10 μs, were mounted 88 cm ab, looking downward. They were stacked

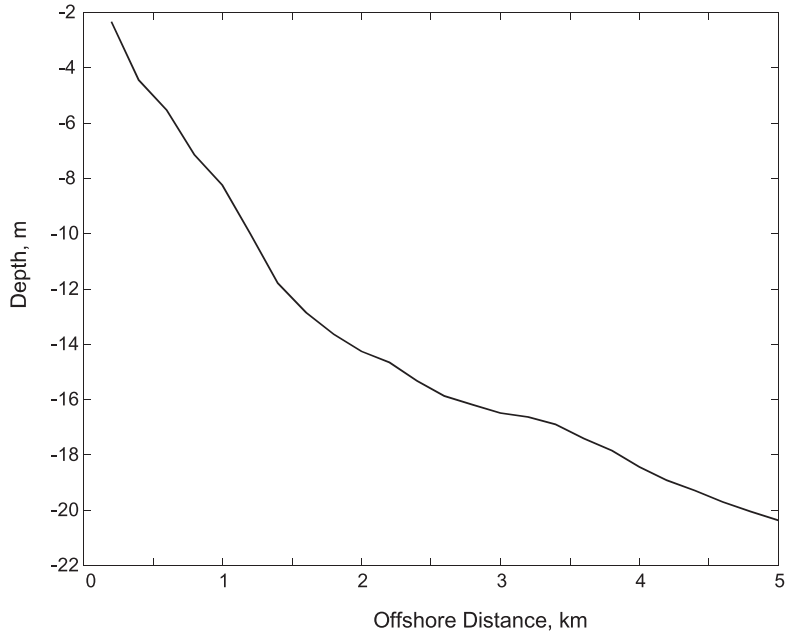

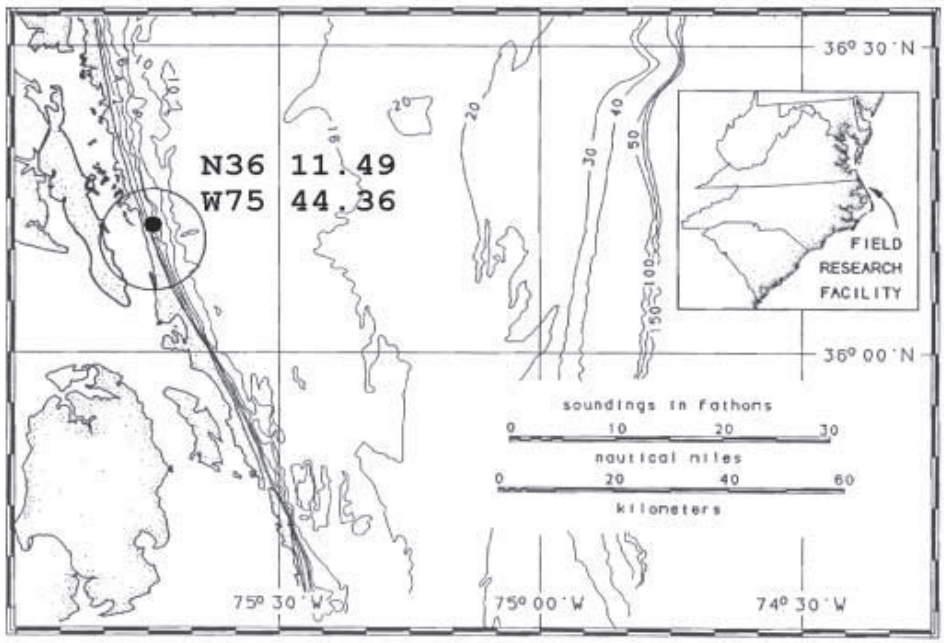

Figure 1. Bathymetry profile and location map of study site. VIMS tripod was deployed at a depth of about 13 m off the Field Research Facility, Duck, North Carolina.

together and thus provided three independent measurements of sediment concentration within less than 5 cm in the horizontal direction. Range gating the backscattered acoustic signal allowed the sediment concentration profile to be estimated at 124 range bins, with a vertical resolution of 1 cm. The pulse repetition rate was 32 Hz and six profiles were averaged before recording the data in the data logger. A detailed description and theory of ABS can be found in the work of *Thorne et al.* [1993]. The ABSs were calibrated in a laboratory resuspension tank at the University of East Anglia using a mixture of sand collected in the sediment trap during the experiment and sand taken from the bottom by divers at the beginning of the experiment. The size distribution of the bed and trap sediment are described in the following section. The backscatter signals at 54 cm below the three ABS transducers were inverted to obtain suspended sediment concentration. Figure 3 shows the comparison of ABS measurement and suction samples at 54 cm below the transducer.

2.3. Environmental Conditions and Characteristics of Observed Suspended Sediment Concentrations

[15] On the third of October 1996, a northeaster developed in the area and lasted ~4 days. During this storm,

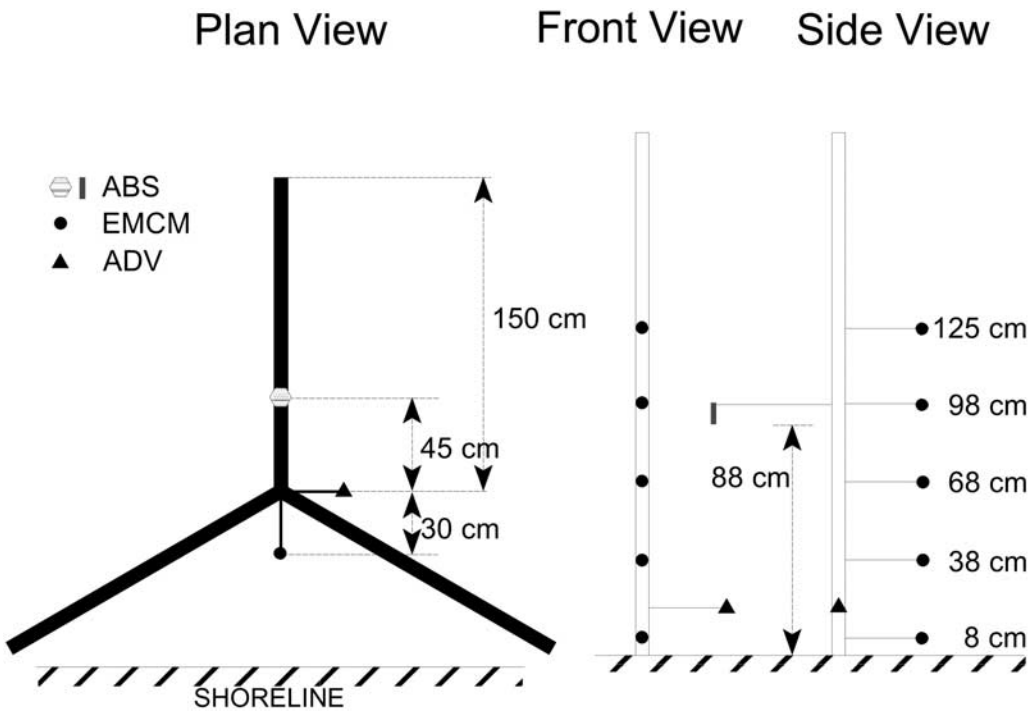

Figure 2. Plan view of VIMS tripod and configuration of instruments.

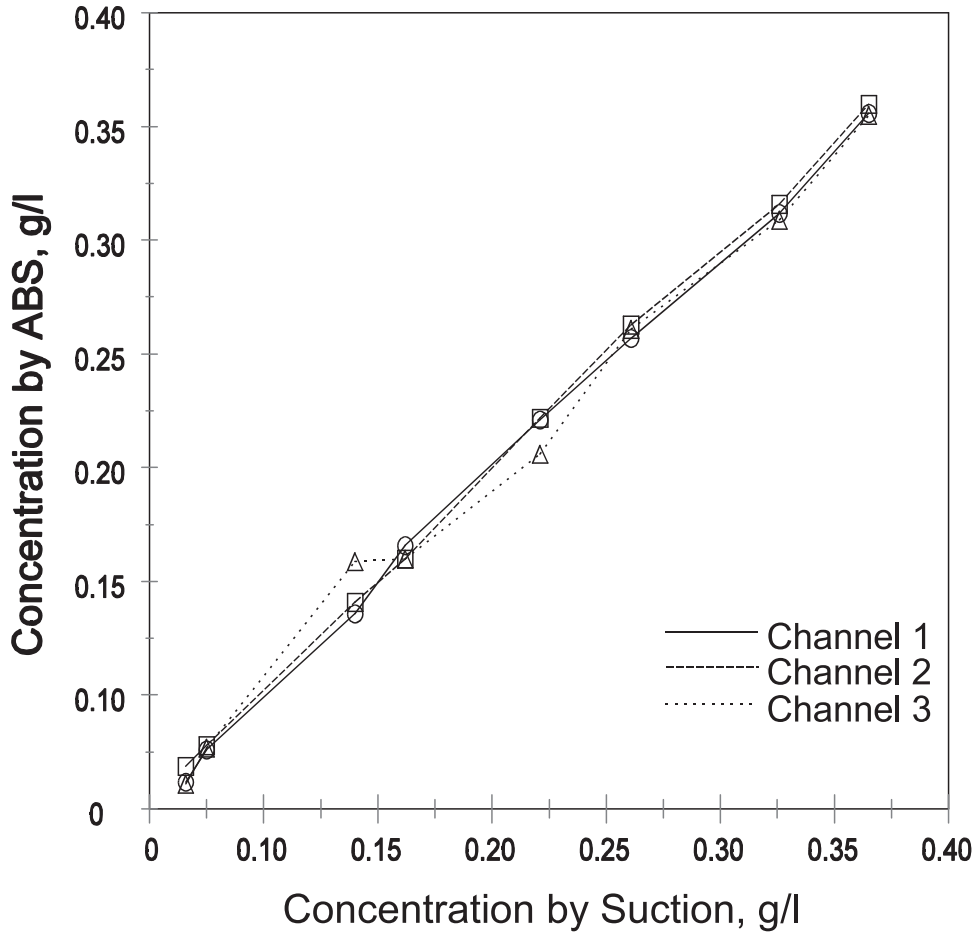

Figure 3. Comparison of concentration by sand suction and acoustic backscatter sensor (ABS) measurement in the University of East Anglia (UEA) calibration tank at a distance of 54 cm from the ABS transducers.

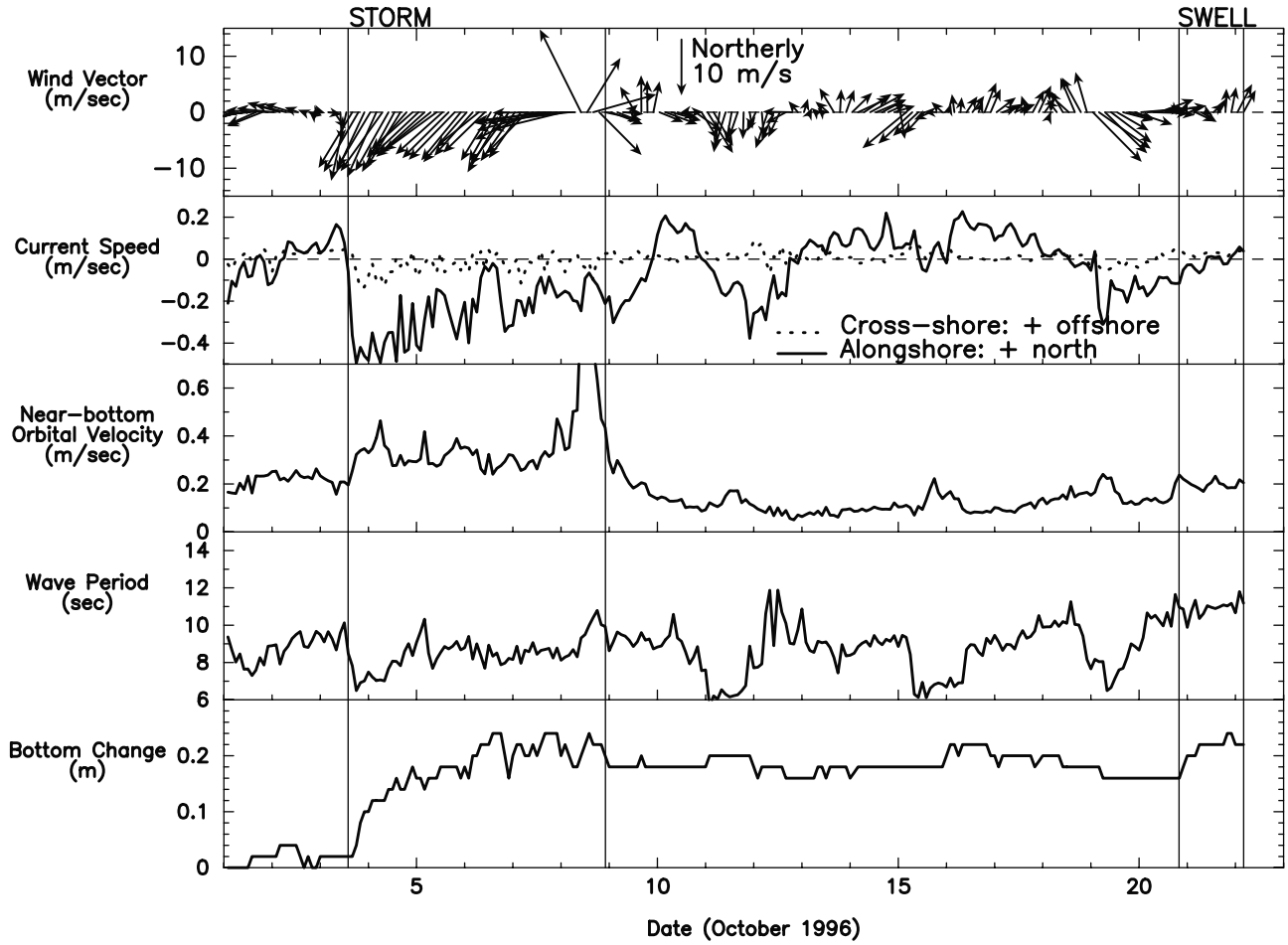

Figure 4. Environmental conditions during VIMS tripod deployment. Storm and swell conditions are delineated by vertical lines. See color version of this figure at back of this issue.

wind speed reached more than 10 m/s and changed its direction to westward as the pressure system passed the area and moved north. The current was predominantly southward along the coast, and its peak speed reached ~50 cm/s at the beginning of the storm and gradually decreased (Figure 4). On 6 October, current speed diminished below 10 cm/s and then increased rapidly to over 30 cm/s on 7 October, gradually decreasing afterward. Near-bottom orbital velocity was ~40 cm/s throughout the storm, and the wave period was ~9 s. Toward the end of the deployment, there was a period of well organized swell. Wave period was ~12 s and near-bottom orbital velocity reached ~30 cm/s. However, current speed was very weak (<10 cm/s) compared to that during the storm. Table 1 tabulates characteristic experimental variables for the storm and swell periods.

[16] Sediment size analyses were performed for a bed sediment core collected by divers at the pod site at the start of the field experiment, and for additional sediment samples obtained in a sediment trap mounted on a leg at 100 cm ab. Both were subsampled at 1-cm intervals, producing 10 and 21 subsamples for bed and trap samples, respectively. Each subsample was divided into sand and silt/clay by wet sieving by following *Folk* [1968]. A Rapid Sand Analyzer was used to measure sand size fractions, while a Micrometrics SediGraph was used to measure silt and clay fractions. Size fractions were almost uniform throughout the core. Table 2 displays the depth-averaged size fractions of the bed sediment. Fine and very fine sands comprised almost 90% and the silt/clay fraction comprised less than 10%. Within the sediment trap (Figure 5), there were two layers for which silt/clay comprised more than 50%: layers ~1 and ~16 corresponding to low-energy periods at the beginning of the experiment and 10–20 October, respectively. The latter distinguishes the swell deposition from the storm deposition. In the swell layers, fine and very fine sands comprised 45 and 14% of the total sediment, respectively. Silt and clay accounted for ~20% of the total sediment and coarser sediment ($<3\phi$) comprised the rest ~20%. The storm layers showed a similar size distribution to the swell layers.

[17] The bed level change was inferred from ABS observations. The level of maximum ABS acoustic backscatter was interpreted as an echo from the bed. This level remained constant (±1 bin, ±1 cm) throughout each burst. Bed level changes observed by the ABS (Figure 4e) exhibit two features: bed form migration and net bed elevation change. During the storm it appears that mega-ripples (O(5–6 cm) in height) passed under the ABSs, whereas smaller ripples (O(2–3 cm) in height) passed under the ABSs during the more quiescent periods. Net accretion on the order of 20 cm occurred during the beginning phase of

Table 1. Statistics of Characteristic Experimental Variables for Storm and Swell Events

	Storm		Swell	
	Mean	Confidence Interval (95%)	Mean	Confidence Interval (95%)
Wind speed, m/s	11.12	0.57	3.32	0.80
H_{mo}, m	2.01	0.09	1.15	0.04
T, s	8.48	0.19	11.23	0.27
u_b, m/s	0.39	0.02	0.27	0.01
u_c, m/s	0.25	0.03	0.04	0.01
log-fit r^2	0.996	0.002	0.969	0.018
predicted η, cm	1.06	0.10	1.27	0.15
predicted λ, cm	10.07	0.37	10.37	0.61
$\delta_{\epsilon s}$, cm	12.12	0.75	11.15	0.66
δ_w, cm	5.23	0.16	5.21	0.18
A_b/k_b	46.92	6.12	36.68	7.09
R	0.46	0.05	2.19	0.33
$u_{*\epsilon s}$, cm/s	2.15	0.53	2.72	0.67
$u_{*\epsilon s}$-fit r^2	0.88	0.03	0.90	0.02
$u_{*c,\mathrm{fit}}$, cm/s	2.11	0.26	0.64	0.16
$u_{*c,\mathrm{model}}$, cm/s	2.06	0.18	0.54	0.08
$u_{*cw,\mathrm{model}}$, cm/s	4.53	0.12	3.45	0.24
abs($u_{*\epsilon s}$-$u_{*c,\mathrm{fit}}$)/$u_{*\epsilon s}$	0.46	0.10	0.75	0.08
abs($u_{*\epsilon s}$-$u_{*c,\mathrm{model}}$)/$u_{*\epsilon s}$	0.32	0.06	0.81	0.04
abs($u_{*\epsilon s}$-$u_{*cw,\mathrm{model}}$)/$u_{*\epsilon s}$	0.90	0.11	0.23	0.10

the storm and in a smaller degree during the storm (O 10 cm). It is uncertain how much of the net accretion is attributable to the tripod settling.

[18] Mean sediment concentrations obtained from the ABS (F2) are shown in Figure 6. Relatively high sediment suspension occurred during the storm and swell, reaching 0.1 g/L at 30 cm above the bottom, while little sediment resuspension occurred during the intervening fairweather conditions. Sediment concentration in the wave boundary layer was significantly higher during the storm than it was during the swell: concentration at 4 cm ab during the storm exceeded about 1 g/L on average, while it was ~0.5 g/L during the swell (Figure 7). However, the storm concentration profile exhibited a faster decay with height than the swell profile (Figure 7). As a result, the concentration at 40 cm ab during the swell was higher than that during the storm. Note that similarly slow decays in concentration with height have been reported by others when waves are present in the absence of strong currents [*Vincent and Osborne*, 1995; *Lee and Hanes*, 1996].

[19] The average concentration profiles for storm and swell with their 95% confidence intervals are shown in Figure 7b. The 95% confidence intervals do not overlap each other except near 30 cm ab where the two average profiles intersect each other. This indicates that they are at least statistically different each other. Further, the accuracy of observed concentration during storm and swell deserves attention. The lowest calibrated concentration was ~0.04 g/L at 55 cm below the transducer (Figure 3). Since the backscattered pressure from a particle in the beam of the ABS transceiver is inversely proportional to the range from the transducer and the mass concentration is proportional to the backscattered pressure squared [*Thorne et al.*, 1993], the accuracy of the ABSs becomes ~0.005 g/L at 20 cm from the transducer. The observed concentrations during the time period of interest exceed 0.005 g/L (see Figures 6 and 7) at 50 cm above the bed, which is equivalent to within 20 cm from the transducer. This indicates that the observed concentrations are within the calibrated range of the ABS accuracy. It could be argued that changes in the dominant grain size of suspended sediment particles during storm and swell conditions might contribute to differences in ABS response during these two periods. However, Figure 5 indicates the suspended material captured in the sediment trap during the storm and swell had a similar grain size distribution. Furthermore, the changes in concentration between storm and swell documented by the three distinct ABS transducer frequencies were highly consistent, which would not be expected if grain size effects were dominating the response.

[20] Observed sediment concentrations also reflect measurement location relative to bedforms. Figure 8 shows concentration time series at 5, 15, and 30 cm ab and bed elevation during storm and swell. Bed elevation change is displayed relative to that at the beginning of the experiment. Higher resuspension was generally observed above bedform crests both during the storm and swell periods. Crests are better resolved by all three ABSs simultaneously during the storm, suggesting the ripples were more sharply crested during the swell than during the storm. During most of the storm the pattern of higher concentration above the bedform crests was no longer evident greater than ~20 cm ab. Similar patterns of significant phase coupling between the

Table 2. Size Fraction of Bed Sediment With $\phi = -\log_2$ (mm)

Sediment Size		Percentage
ϕ	Millimeter	
<2	>0.25	0.69
2 ~ 2.5	0.25 ~ 0.177	1.90
2.5 ~ 3	0.177 ~ 0.125	29.15
3 ~ 3.5	0.125 ~ 0.088	60.03
3.5 ~ 4	0.088 ~ 0.063	2.84
4 ~ 6	0.063 ~ 0.015	3.23
>6	<0.015	2.16

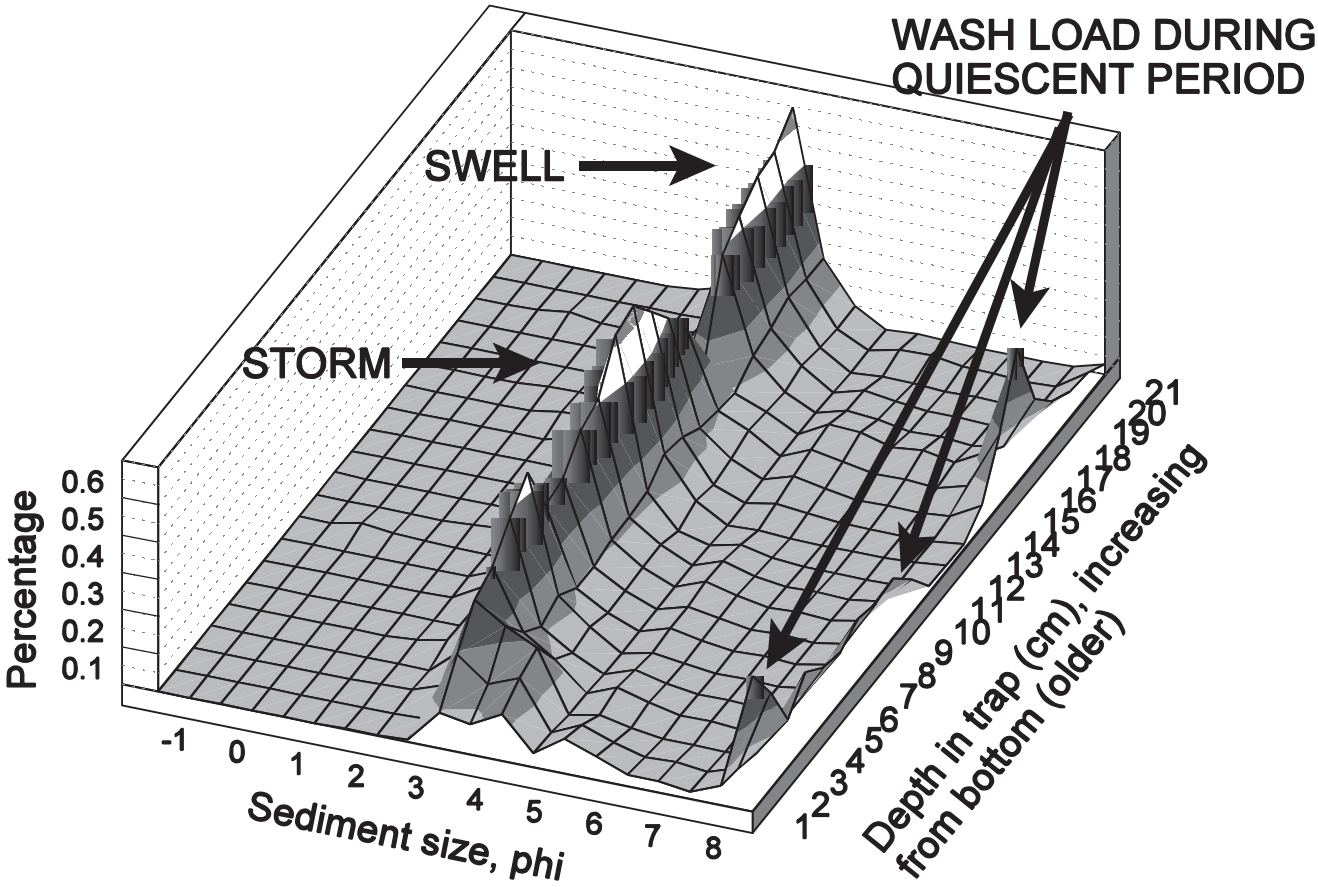

Figure 5. Sediment size fractions of trap sediment. A significant increase in percent fine sediment deposition is seen between coarser storm and swell deposits. See color version of this figure at back of this issue.

resuspended sediment and the bedforms in the near bed region (<10 cm ab) and less significant coupling above that level have also been observed on a macrotidal beach in the U.K. [*Osborne and Vincent*, 1996]. In contrast, during the majority of the swell period in Figure 8, high concentration above bedform crests extended more than 30 cm ab. This is because, as described above, waves during the storm did not appear to eject sediment as high into the water column as they did during swell.

[21] It is important to note the possibility that the configuration of the tripod may have affected the vertical distribution of sediment concentration. Our greatest concern is that sediment plumes scoured by the pod's legs may have advected past our instruments. During the storm when currents were strong, the direction of horizontal suspended sediment advection would have been predominantly south, in which case the disturbance from pod to the ABS might have been minimal (see Figure 2). During weak current conditions, sediment movement would have been predominantly on/offshore aligned with the shore normal wave direction. Thus disturbance associated with the offshore leg might have been detectable at the center post. This effect might have been exaggerated during low current conditions when periodic wave motion might have advected scoured sediment back and forth under the pod. This could conceivably account for a steepened concentration profile under swell conditions. An indication of severe scour nearby might be a reversed concentration profile: higher concentrations at higher height. The concentration data showed no such events, except for minor fluctuations consistent with random variations.

3. Eddy Viscosity and Eddy Diffusivity

[22] In order to obtain the linearly increasing eddy viscosity profiles specified by equation (4), characteristic shear velocities must be determined. To do so here, two methods were applied: the best-fit log profile and a wave-current interaction model. The best fit log profile method involves estimating the shear velocity from the mean current profile within the current boundary layer utilizing the law of the wall

$$u_c = \left(u_{*_c}/\kappa\right)\ln(z/z_{oc}), \tag{10}$$

where u_c is the time averaged flow velocity at a height, z, and z_{oc} is the z intercept at which u_c becomes zero.

[23] A second method for estimating the shear velocity is via a wave-current interaction model. Wave-current interaction models are usually used to predict u_{*c} and z_{oc}, apparent roughness, values defining the current profile above the wave boundary layer, from knowledge of current

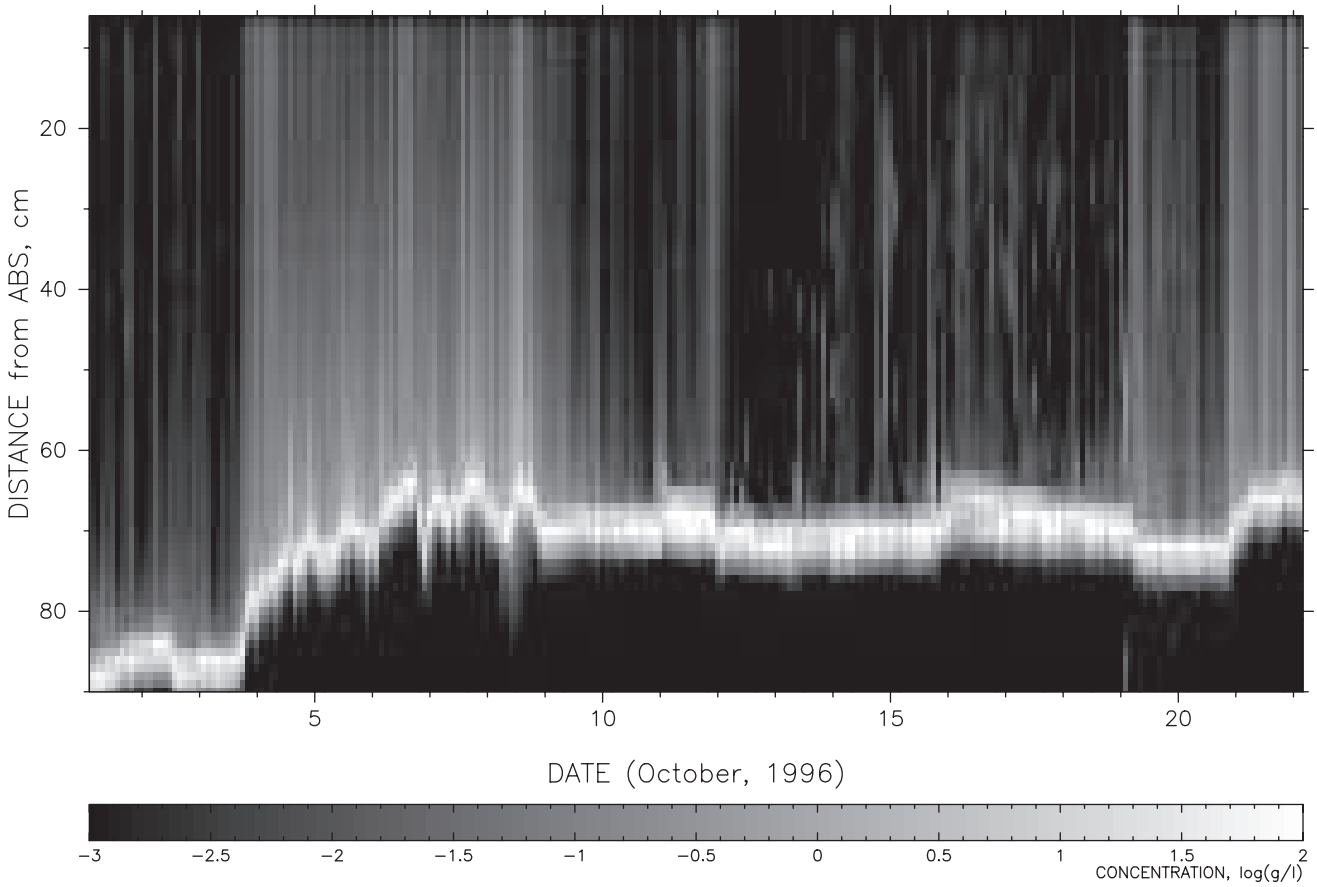

Figure 6. Burst-averaged sediment concentration during the deployment. Relatively high sediment suspension occured during the storm (4–8 October, 1996) and swell (20–21 October), but virtually no suspension occured during the fairweather condition (10–20 October). Bed elevation relative to the sensors increased by ~20 cm during the storm. See color version of this figure at back of this issue.

at a point, near-bottom wave orbital velocity and physical bottom roughness characteristics. The Grant-Madsen-Glenn [*Grant and Madsen*, 1986; *Glenn and Grant*, 1987; hereinafter referred to as GMG] wave-current interaction model was applied because this model uses a strictly linear eddy viscosity model. In addition, it is relatively simple and has been widely applied in the literature. This model also provides the shear velocity owing to waves and the shear velocity owing to the combined effect of waves and current in the wave boundary layer [*Grant and Madsen*, 1986]. Other models use slightly more complicated, continuous profiles for viscosity [e.g., *Smith*, 1977; *Madsen and Wikramanayake*, 1991]. Viscosity within these other models is asymptotic to equation (4) with portions of the wave and current boundary layer. The ultimate result for predicted sediment concentration is not sensitive to the difference in these authors' viscosity formulation.

[24] To apply the GMG model, total bed roughness was defined as

$$k_b' = k_b + k_{br} + k_{bm}. \tag{11}$$

The grain roughness, k_b, is on the order of grain diameter ($2.5d_s$, where d_s= 0.017 cm is the mean sediment size in the bed) and the drag roughness, k_{br}, used the relationship given by *Nielsen* [1992] in terms of ripple geometry

$$k_{br} = 8\eta(\eta/\lambda), \tag{12}$$

where η is the ripple height and λ is the ripple length. Ripple height and length were estimated using the *Wiberg and Harris* [1994] wave-generated ripple model. The ripple model divides the bedforms into orbital, suborbital, and anorbital ripples by a function of grain size and wave orbital diameter d_o. The criteria to determine ripple types are

$$\text{Orbital ripples} \qquad d_o/\eta_{\text{ano}} < 20, \tag{13a}$$

$$\text{Anorbital ripples} \qquad d_o/\eta_{\text{ano}} > 100, \tag{13b}$$

$$\text{Suborbital ripples} \qquad 20 < d_o/\eta_{\text{ano}} < 100, \tag{13c}$$

where η_{ano} is the anorbital ripple height. The height of anorbital ripples can be estimated by using the relationship

$$\eta/\lambda = \exp\left[-0.095\left(\ln\frac{d_o}{\eta}\right)^2 + 0.442\ln\left(\frac{d_o}{\eta}\right) - 2.28\right]. \tag{14}$$

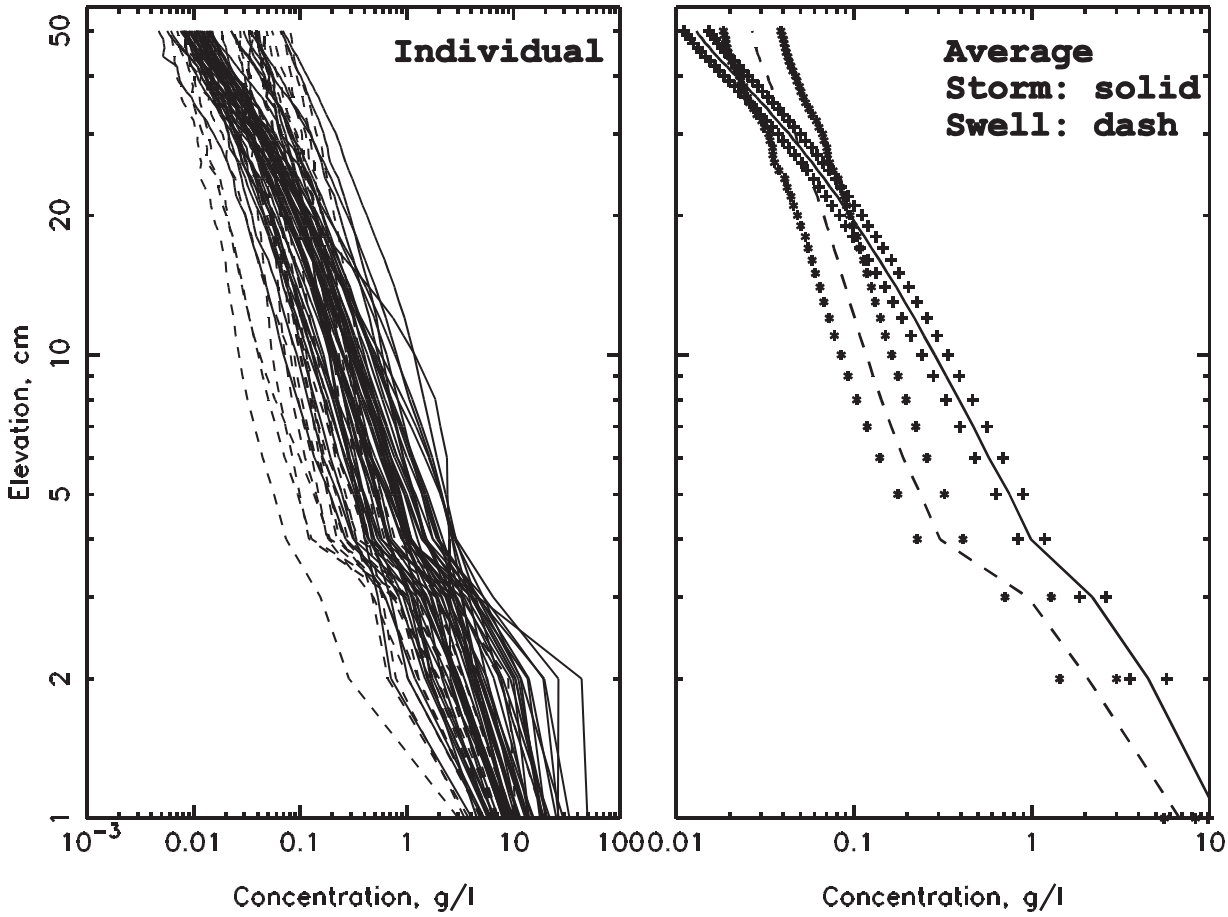

Figure 7. Average sediment concentration profile during the storm and swell. Plus and asterisks indicate 95% confidence interval of storm and swell average sediment concentration profiles, respectively. Near-bottom sediment concentration during the storm was higher (by a factor of 2) than during the swell. However, the concentration gradient (decay rate) with elevation was greater during the storm. See color version of this figure at back of this issue.

The orbital wavelength is $\lambda_{\text{orb}} = 0.62 d_o$, and all orbital ripples are defined as having a steepness of 0.17. The suborbital wavelength is defined by

$$\lambda_{\text{sub}} = \exp\left[\left(\frac{\ln(d_o/\eta_{\text{ano}}) - \ln 100}{\ln 20 - \ln 100}\right)(\ln \lambda_{\text{orb}} - \ln \lambda_{\text{ano}}) + \ln \lambda_{\text{ano}}\right]. \quad (15)$$

The height of suborbital ripples is estimated iteratively using equations (14) and (15). The anorbital wavelength is $\lambda_{\text{ano}} = 535 d_s$. The *Wiberg and Harris* [1994] ripple model predicted ripples to be predominantly anorbital during the storm and transitional between anorbital and suborbital during the swell. Unfortunately, we were not equipped to measure bedform geometry, and it is impossible to examine the accuracy of the model with only the change of bed level observed at a point by the ABSs.

[25] Movable bed roughness due to sediment transport, k_{bm}, was estimated by following *Xu and Wright* [1995]

$$k_{bm} = 5\left(\tau'_{sf} - \tau_{cr}\right)/[(\rho_s - \rho)g], \quad (16)$$

where ρ_s and ρ are densities of the sediment and fluid and g is acceleration of gravity. The skin friction shear stress τ_{sf}' is defined by

$$\tau'_{sf} = 1/2\rho f_{cw} u_b^2, \quad (17)$$

where f_{cw} is the friction factor given by *Madsen and Wikramanayake* [1991]. The critical stress for initiation of motion is $\tau_{cr} = 0.15$ Pa for $d_s = 0.012$ cm [*Dyer*, 1986]. Figure 9 displays the predicted contributions to k_b' from the three roughness components through the storm and swell events.

[26] Figure 10 shows typical eddy diffusivity and eddy viscosity profiles estimated as described above during storm and swell events. Apparent eddy diffusivity profiles were estimated independently using each of the three ABS channels by

$$\epsilon_s = w_s C/(\partial C/\partial z), \quad (18)$$

where $w_s = 1.0$ cm/s for $d_s = 0.012$ cm [*Dietrichs*, 1982]. The concentration gradient, $\partial C/\partial z$, was calculated for successive height intervals of 1 cm. Eddy viscosity profiles were calculated by using equation (4) with shear velocities

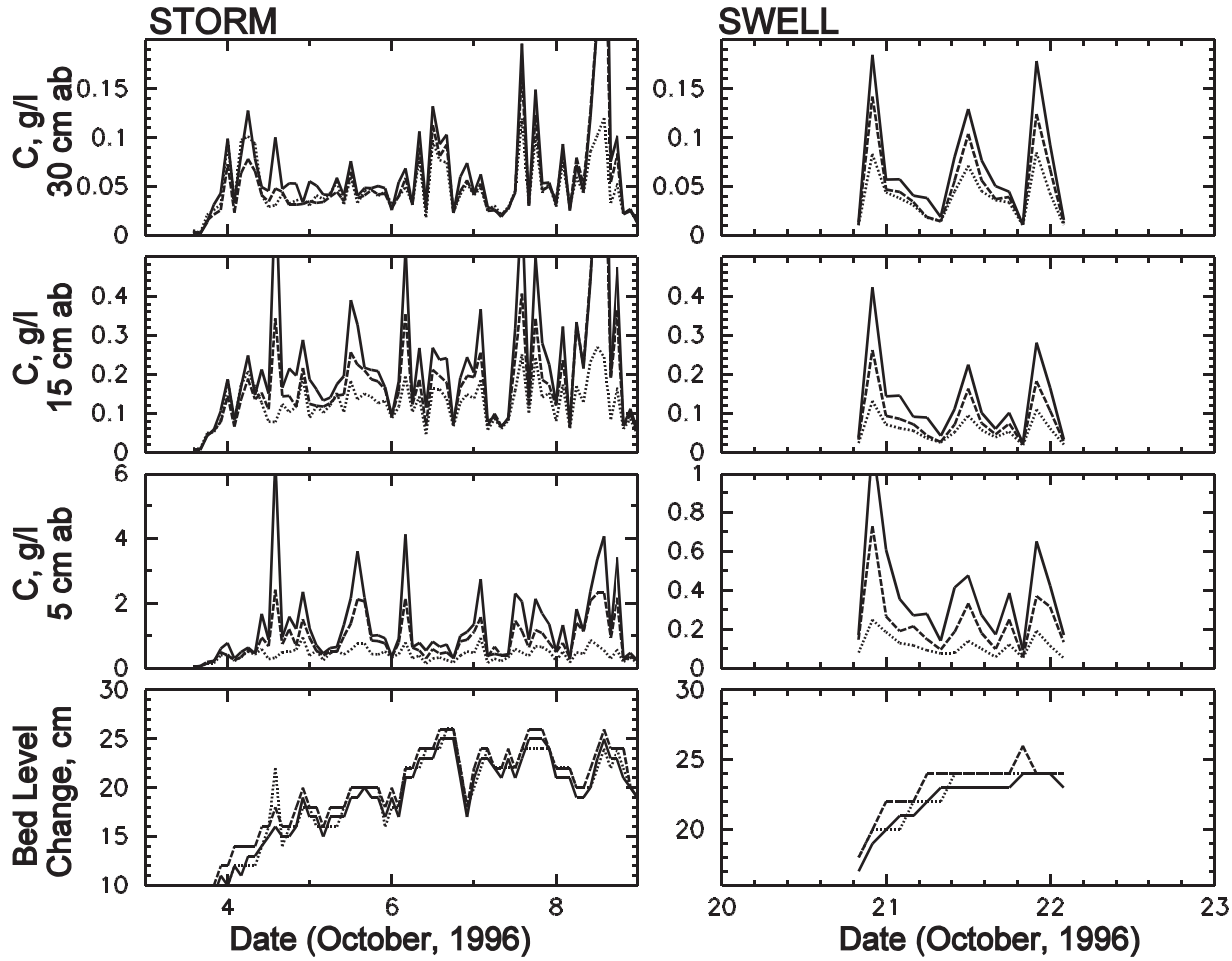

Figure 8. Observed sediment concentration at 5, 15, and 30 cm ab and observed bed level change during (left) storm and (right) swell. Higher resuspension above bedform crests is inferred for both storm and swell. A vertically coherent pattern of higher concentration above bedforms continues up to ~20 cm during storm and above 30 cm during swell. Above 20 cm ab during the storm, higher concentration does not necessarily correspond to bedform location, suggesting a different vertical mixing mechanism is at work. Solid line, F1; dash, F2; dot, F3. See color version of this figure at back of this issue.

obtained by (1) a log-linear fit to the observed burst-averaged current profile ($u_{*c,\mathrm{fit}}$) and (2) the GMG model as described above ($u_{*\mathrm{model}}$). Under storm conditions the vertical structure of eddy viscosity (ϵ_m) associated with the log-fit shear velocity was consistent with diffusivity (ϵ_s) calculated by equation (18) up to a maximum of ~20 cm ab. Above the linear region, the diffusivity profile exhibited a less consistent structure. Nonetheless, ϵ_m associated with u_{*c} still provided an upper bound on observed ϵ_s. Note that eddy viscosity profiles estimated by a log-linear fit and modeled by the GMG agree well. Under swell the vertical structure of ϵ_s was consistent with ϵ_m within the wave boundary layer. Above the wave boundary layer, ϵ_s diverged from ϵ_m associated with u_{*c} but continued to increase as if still determined by the higher shear velocity (u_{*cw}) predicted by the GMG model within the wave boundary layer. Similar to the storm diffusivity profile, the swell diffusivity profile exhibited a less coherent structure above ~20 cm ab.

[27] Figure 11 displays time series of shear velocities during storm and swell. Shear velocity associated with eddy diffusivity ($u_{*\epsilon s}$) was inferred via a least squares fit to the linearly increasing eddy diffusivity profiles of ABS F2 using equation (4). The maximum height of the linearly increasing eddy diffusivity for purposes of curve fitting was determined by two criteria. Either the difference of eddy diffusivity between two consecutive levels was greater than 10 cm^2/s or there were more than two consecutive, negative values. It is noted that we also attempted to obtain a distinct value for shear velocity based on the eddy diffusivity profile entirely within the WBL as predicted by the GMG model. However, the estimates were unreliable owing to high scatter and too few data points. As described above, $u_{*\varepsilon s}$ agreed well with u_{*cw} during swell and with $u_{*\mathrm{c}}$ most of the time during the storm. Table 1 displays r^2 values during storm and swell for the log-linear fit to the mean current profile and also the linear fit to the eddy diffusivity profile. Table 1 also contains statistics for the observed upper limit of the linearly increasing eddy diffusivity layer ($\delta_{\varepsilon s}$) and the degree of agreement between the shear velocity associated with eddy diffusivity ($u_{*\varepsilon s}$) and other estimates of u_* in terms of the average absolute difference, abs($u_{*\varepsilon s}$ - u_*)/$u_{*\varepsilon s}$, for storm and swell. During the storm, eddy diffusivity was

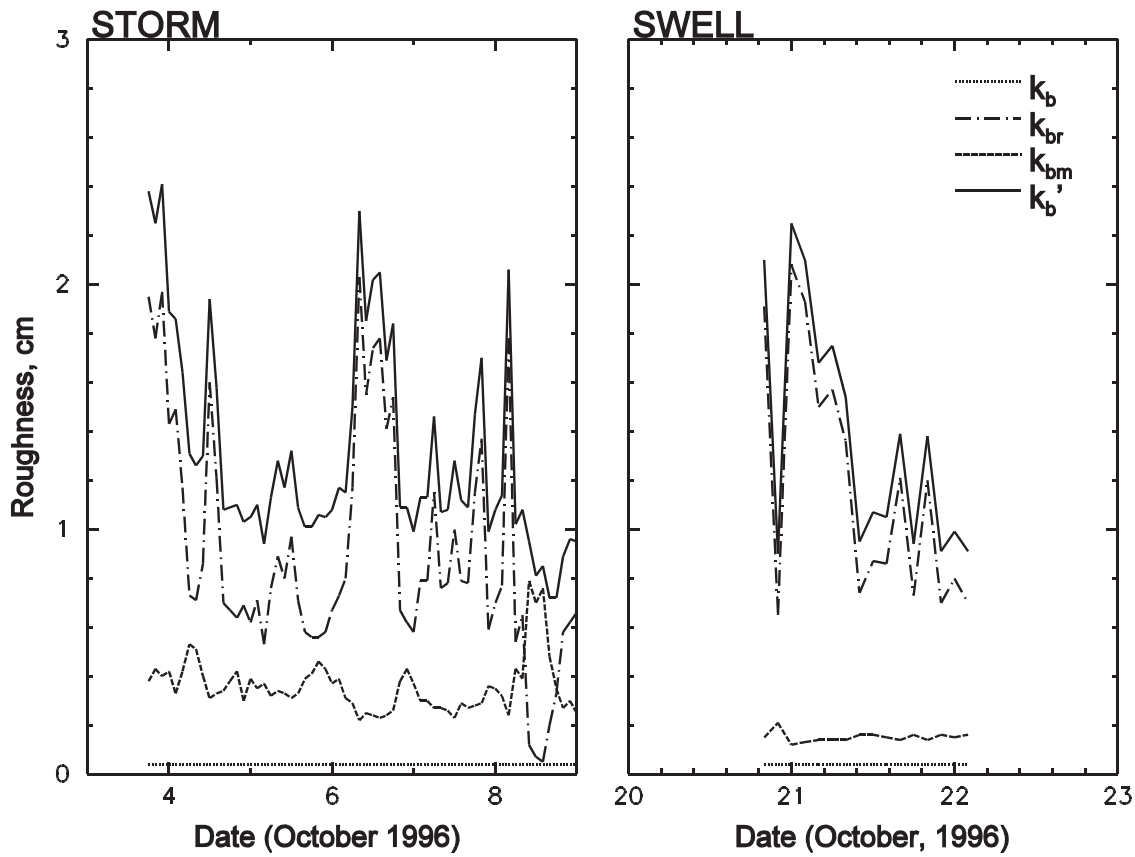

Figure 9. Modeled bed roughness during (left) storm and (right) swell. The k_b value is grain roughness, k_{br} is drag roughness due to ripples, k_{bm} is movable bed roughness, and k_b' is total roughness. See color version of this figure at back of this issue.

more consistent with u_{*c}, whereas during the swell, eddy diffusivity was more consistent with u_{*cw}.

4. Diffusion-Dominated Vertical Distribution of Suspended Sediment

[28] In this section, the two layered Rouse model of *Glenn and Grant* [1987] for suspended sediment distribution is applied to the above storm and swell dominated observations. The two-layered Rouse model is obtained by integration of equations (3) using (4) below and above the WBL, neglecting sediment induced stratification:

$$C_{zi} = C_{ri}(z/z_o)^{-w_{si}/\kappa u_{*cw}} \qquad z \le \delta_w \qquad (19a)$$

$$C_{zi} = C_{ri}(\delta_w/z_r)^{-w_{si}/\kappa u_{*cw}}(z/\delta_w)^{-w_{si}/\kappa u_{*c}} \qquad z > \delta_w, \qquad (19b)$$

where C_{zi} and C_{ri} are the concentrations at height, z, and at a reference height, z_r, respectively and the subscript i indicates the ith size class. The reference concentrations are given as

$$C_{ri} = \gamma_o C_b \left(\frac{\tau'_{sf} - \tau_{cri}}{\tau_{cri}}\right), \qquad (20)$$

where γ_o is the resuspension coefficient, C_b is the volume concentrations in the bed sediment, and τ_{cri} is the critical shear stresses for initiation of motion. Following *Webb and Vincent* [1999], the observed resuspension coefficients were correlated against maximum skin-friction Shield parameters, θ' (Figure 12). Values of the Shields parameters were calculated by

$$\theta' = \left(\frac{\tau_{sf}'}{\rho(s-1)gd_s}\right), \qquad (21)$$

where s = 2.65 is the density of quartz relative to water. The observed resuspension coefficient was calculated by inverting equation (20) with reference concentration matching with observed concentration at 1 cm above the bed. The regression of $\log(\gamma_o)$ on $\log(\theta')$ was significant at 99%, giving $\gamma_o = 4.3 \times 10^{-4}\ (\theta')^{-1.44}$.

[29] Seven grain sizes, shown in Table 2, were used to reproduce the distribution observed in the bed. Following *Wiberg et al.* [1994], bed armoring was incorporated into the model to limit sediment suspension of especially fine fractions to not more than the available sediment in the bed. In order to limit excessive sediment suspension, total suspended sediment, predicted by equation (19) for each size fraction, was integrated from the bed to half the water depth and was compared to the available sediment for each fraction above the mixing depth. If the total suspension of a fraction exceeded the available sediment in the bed, the reference concentration for that fraction was reduced until

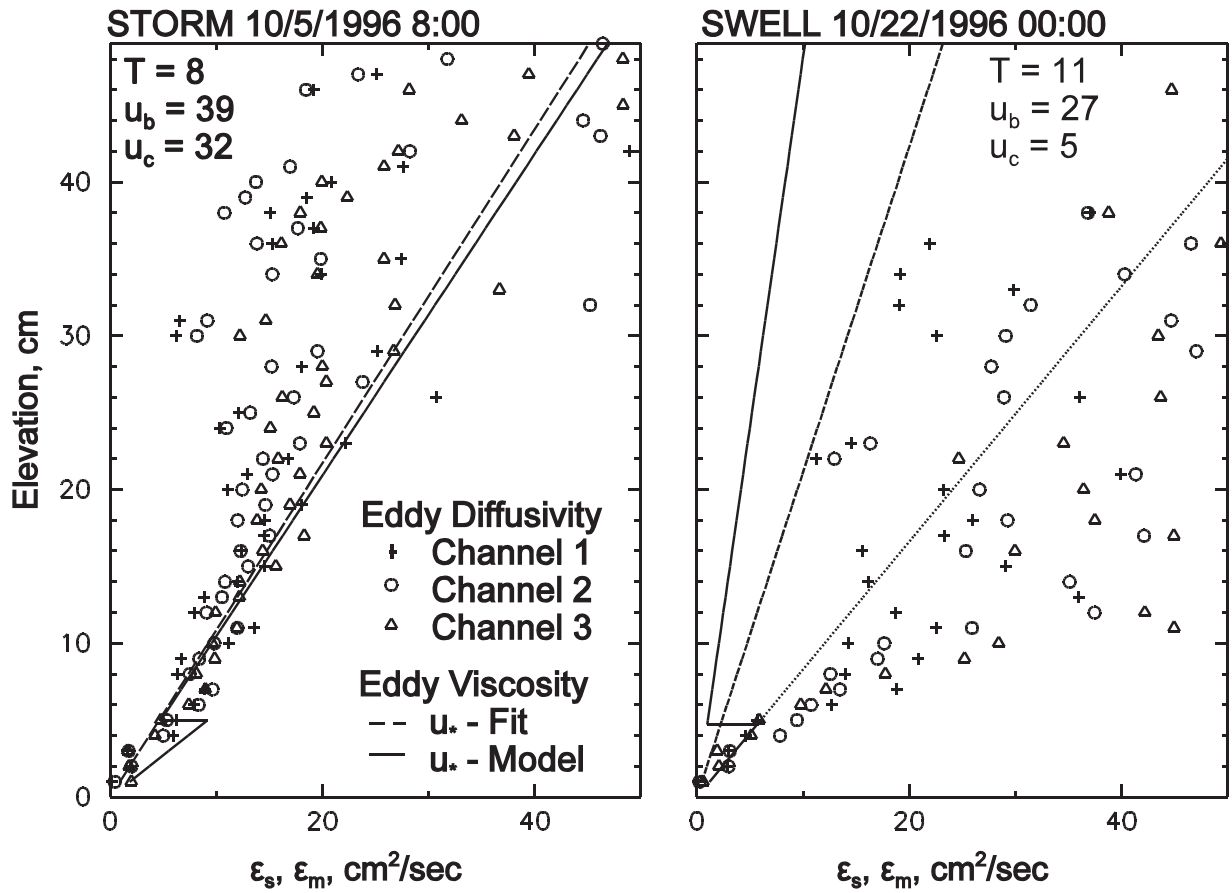

Figure 10. Eddy viscosity and diffusivity profiles during (left) storm conditions on 5 October 1996 at 0800 UT and (right) swell conditions on 22 October 1996 at 0000 UT. The $u_{*\mathrm{fit}}$ is from the observed current profile, and $u_{*\mathrm{model}}$ is predicted by the Grant-Madsen-Glenn (GMG) model. Eddy viscosity using u_{*cw} above the wave boundary layer is shown by a dotted line for the swell case. Wave period T, current speed at 1 m ab u_c, and near-bottom orbital velocity u_b are also shown. See color version of this figure at back of this issue.

the total suspended sediment of that size no longer exceeded the amount available in the bed. The mixing depth is defined as the maximum depth to be eroded at a certain flow condition and is given by

$$\delta_m = q_{bl}T/(C_b\lambda) + \delta_b, \tag{22}$$

where δ_m is mixing depth, q_{bl} is bedload transport rate, and T is wave period. The δ_b value represents a background mixing depth, set to 1 mm [*Wiberg et al.*, 1994]. This is useful when flow conditions are so weak that there is no bed load transport, but fine sediment can be removed from the mixed sediment. The bedload transport rate was estimated from the *Meyer-Peter and Müller* [1948] equation, $q_{bl} = 8(\tau' - \tau_{\mathrm{cr}})^{1.5}/(\rho_s - \rho)g$.

[30] Figure 13 shows the vertical distribution of suspended sediment from the bed level to 50 cm above the bottom during storm and swell conditions. The example bursts are the same as those used in Figure 10. The two-layered Rouse model reproduced the storm data quite well, while it considerably underestimated concentration above the wave boundary layer during swell conditions. This is consistent with the results for apparent eddy diffusivity (ϵ_s): the GMG model reproduced ϵ_s above the WBL well during the storm, whereas the model significantly underestimated ε_s as derived from equation (18) during swell. The modeled concentrations for a two-layered Rouse-type model with no bed armoring clearly show the reason why the bed armoring must be included in order to limit the sediment suspension of fine fractions. Because of very low settling velocity of fine sediment, the concentration is highly unrealistic. For comparison, the results for a two-layered Rouse-type model with single, mean grain size, for which armoring effect was not incorporated, are also shown in Figure 13. The degree of agreement between the observed (C_{obs}) and modeled (C_m) concentrations was calculated in terms of the average absolute difference, abs$(C_m - C_{\mathrm{obs}})/C_m$, at 5 and 30 cm above the bed during storm and swell conditions and is shown in Table 3. Also shown in Figure 13 are the results for a three-layer Rouse model, which incorporates the intermediate constant viscosity layer of *Madsen and Wikramanayake* [1991]. The intermediate layer allows the viscosity profile to remain continuous, which is important for implementation of *Nielsen*'s [1992] advection component later in this paper. As shown in Figure 13, the time-averaged concentration profile predicted by diffusion alone is insensitive to this modification. In contrast, it is noted that multiple grain size in combination with bed armoring

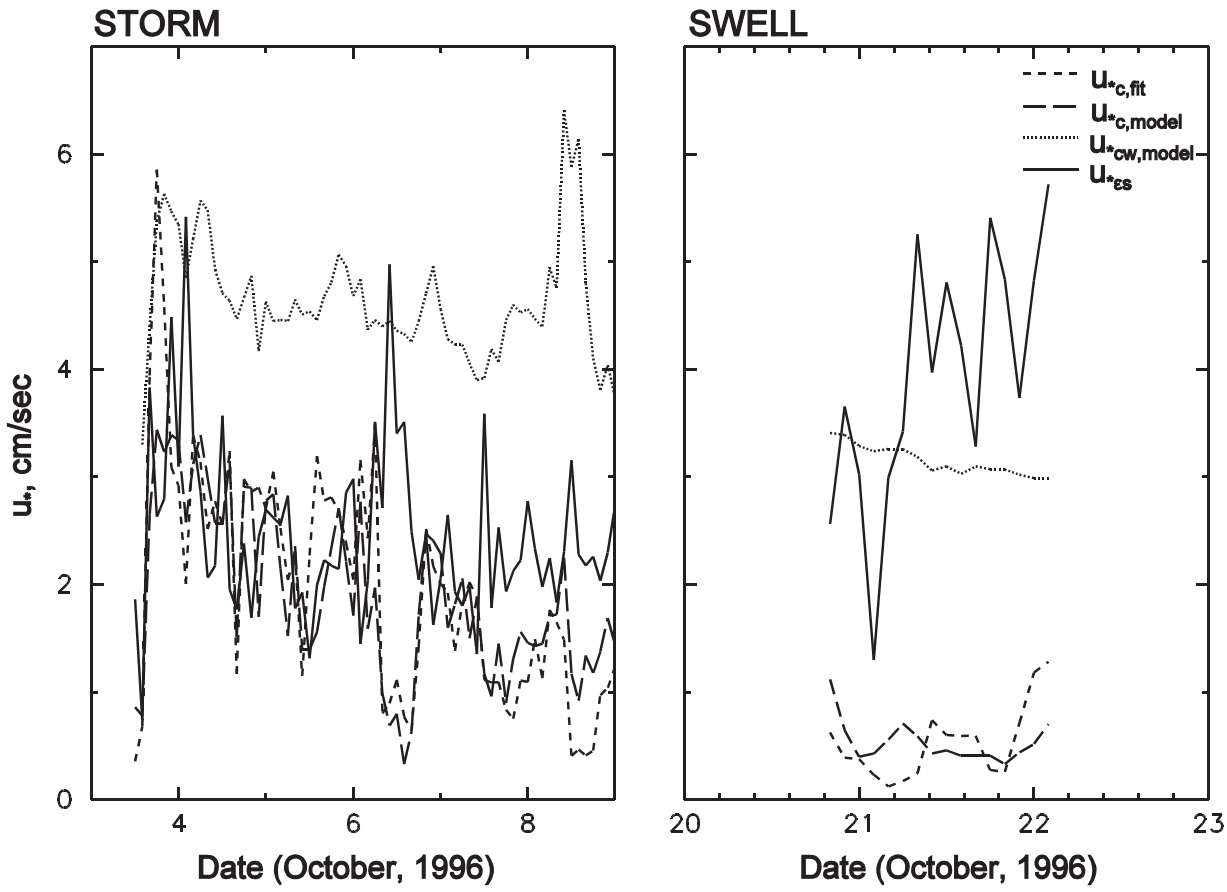

Figure 11. Time series of shear velocities during (left) storm and (right) swell.

[*Wiberg et al.*, 1994] greatly improved the model results above the WBL during storm conditions relative to the results for a single grain size or seven grain sizes without armoring (Table 3). However, none of the models in Figure 14 were able to reproduce observed concentration above the WBL during swell conditions.

[31] Figure 14 displays time series of observed and modeled sediment concentrations at 5 and 30 cm above the bed during storm and swell conditions. The bursts for which the Rouse model failed to reproduce the observations above the wave boundary layer are hatched, signifying that the assumption of equality between model predicted eddy viscosity and observed apparent eddy diffusivity was invalid. These periods when shear velocity inferred from apparent diffusivity ($u_{*\epsilon s}$) follows WBL shear velocity (u_{*cw}) included most of the swell cases as well as several bursts during the storm on 6 October. The physical mechanisms associated with these two distinct suspension modes are discussed in the following section.

5. Criteria for Diffusion Versus Advection-Dominated Sediment Suspension

[32] In the previous section, we showed that the assumption of equation (4), equality of observed ϵ_m and modeled ϵ_s, was valid during most of the storm event but was invalid during swell and during a few storm bursts. In order to further examine under what conditions the assumption of equation (4) was invalid, we introduce a scaling parameter R, which is the ratio of the vertical advection velocity relative to the mean current, $u_{c,\delta}$ at the top of the GMG wave boundary layer. Here, the vertical advection or "jet" velocity, u_j, is scaled to $(\eta/\lambda)u_b$, where η and λ are the modeled ripple height and ripple length, respectively, and u_b is the maximum near-bottom orbital velocity. *Andreapoulos and Rodi* [1984] performed laboratory experiments on near-bed jets impinging on a mean current. They found that at small ratios of jet-to-cross flow velocity ($R < \sim 0.5$), the jet was immediately bent over by the cross flow, while at higher R values ($R > \sim 0.5$) the jet penetrated farther into the cross flow. The results of Andreapoulos and Rodi can be applied to vortex shedding by waves over ripples under a mean current. Following their argument, at small R values, turbulent diffusion by mean current shear outside the classical wave boundary layer should be the dominant process of vertical mixing because the current itself will block the jets associated with ripple vortex shedding. For cases of higher R value the current will no longer block the vortices and suspension above the classical WBL should be supported by vertical advection associated with vortex shedding.

[33] Figure 15a displays a time series of the scaling parameter R. In addition, wave orbital velocity and current velocity are shown in Figure 15b. Figure 15c displays u_{*cw}, $u_{*c,\mathrm{model}}$ and $u_{*cr} \approx w_s$ for the mean sediment size, where u_{*cr} is the critical shear velocity for suspension. Periods with $R > 1.0$ generally correspond to times when the

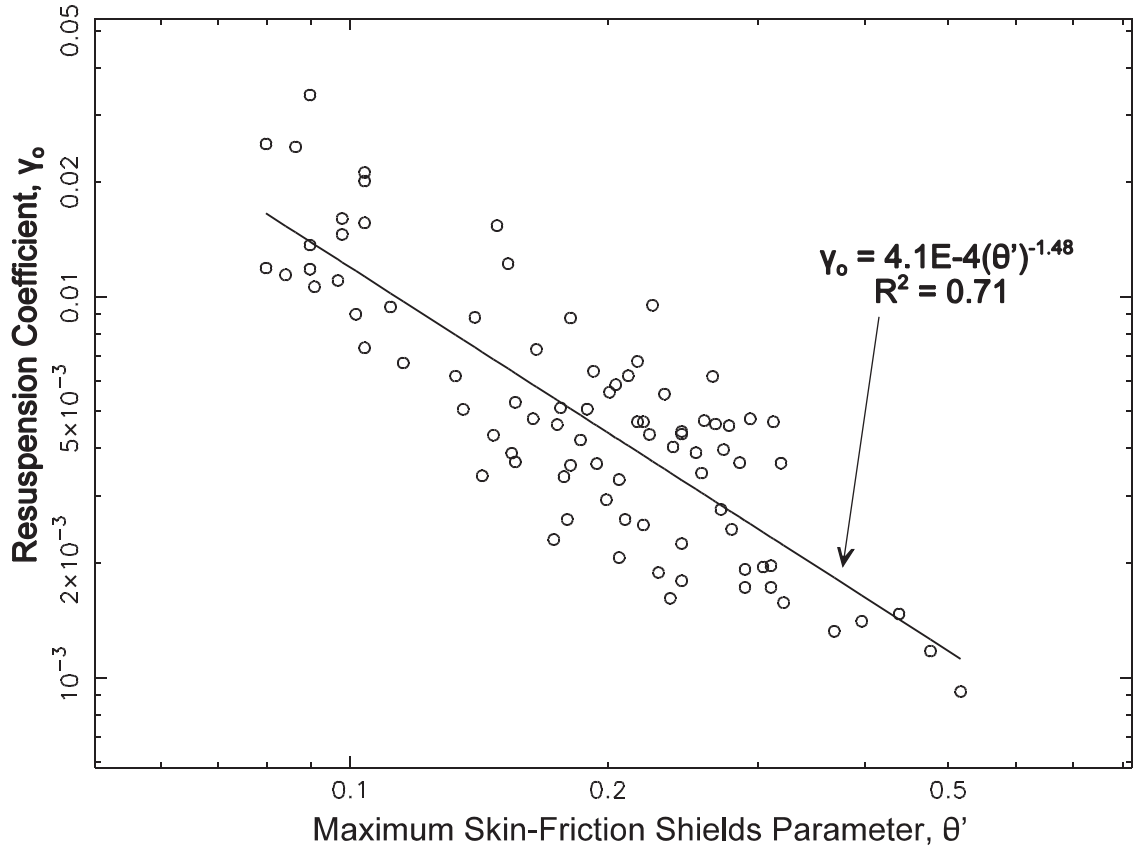

Figure 12. Plot of resuspension coefficient as a function of skin-friction Shields parameter. The regression fit is also shown as the solid line.

assumption of equation (4) failed (see Figure 15). This pattern is consistent with the observations of jet penetration by *Andreapoulos and Rodi* [1984]. The periods of higher R values ($R > 1.0$) correspond to weak currents (cross flow less than 10 cm/s), and waves strong enough to suspend sediment from the bed (Figure 15b). Interestingly, when R was greater than 1.0, u_{*c} was usually smaller than the fall velocity of the sediment (Figure 15c). The weak currents enabled the shedding vortices to penetrate farther above the predicted wave boundary layer, while turbulence associated with the mean current was simultaneously too weak to maintain sediment in suspension. Smaller values of $R < 1.0$ corresponded to strong current conditions when the associated shear was greater than w_s. Thus the dominant process for $R < 1.0$ was sediment diffusion associated with current-generated turbulence outside the wave boundary layer. Somewhat paradoxically, the strong current actually reduced mean sediment concentration 40 cm ab relative to swell conditions by blocking the sediment-laden jet penetration.

6. Combined Diffusion and Advection Model of Vertical Distribution of Suspended Sediment

[34] In section 5, a diffusion-based model was used to solve equation (3) for the time-averaged suspended sediment distribution. The diffusion-gravitational settling balance appeared to be a good approximation close to the bed during the storm when turbulent diffusion associated with a strong mean current was a dominant process. However, this balance as formulated by the GMG model did not appear to hold when the current was weak but wave energy was still strong enough to suspend sediment from the bed. In this section, we apply *Nielsen*'s [1992] combined diffusion and advection model (7). The integration of equation (7) with equations (6), (8), and $P = w_s C_{ri}$ yields

$$C_{zi} = C_{ri}\, e^{-w_{si}z/\varepsilon_s}\left(\frac{w_{si}}{\varepsilon_s}\int_0^z \frac{e^{w_{si}z'/\varepsilon_s}}{\left(1+11z'\left(k_b' A_b\right)^{-1/2}\right)^2}dz' + 1\right). \tag{23}$$

C_{ri} was determined by equation (20) along with armoring effects as described in section 5.

[35] Suspended sediment concentrations predicted by the combined diffusion and advection model are shown in Figure 16, along with the observed concentrations and the predicted concentrations using the Nielsen model with advection turned off. Although the combined model reproduced the swell data better than either the Rouse model (see Figure 13) or the Nielsen model without advection turned off, the combined model still underestimated the observed concentrations. Furthermore, it significantly underpredicted the storm data (see also Table 3). This appears to result from the adoption of the constant eddy

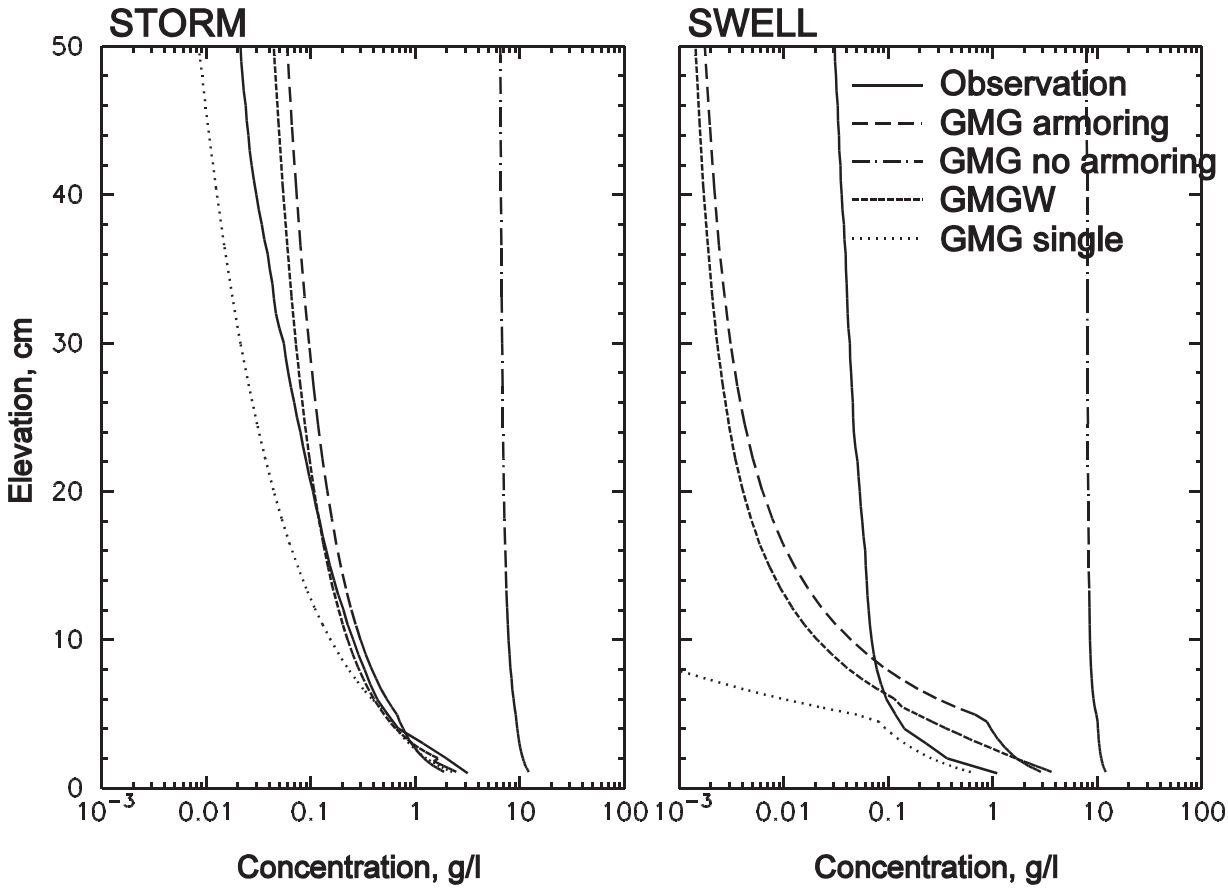

Figure 13. Observed (F2) and modeled sediment concentration profiles during (left) storm and (right) swell. Two-layered GMG [*Glenn and Grant*, 1987] and three-layered GMGW [*Madsen and Wikramanayake*, 1991] Rouse-type models were used to model suspended sediment concentration. The GMG single is the only model run which used a single grain. The GMG single and GMG no armor are the only model runs that did not include the bed armoring.

diffusivity. Eddy diffusivity estimated by equation (8) gave small values throughout the water column, O(1 cm^2/s). This may be a reasonable estimation very near the bed, but effective ϵ_s was observed to be an order of magnitude larger at 10–20 cm ab (see Figure 10). Arguably, the storm conditions are outside the wave-dominated regime intended for the Nielsen model, since mean currents during the storm were significant.

[36] In section 5, it was observed that effective eddy diffusivity increased linearly in the near-bottom region not only during the storm but also during swell conditions. Thus it is appropriate to examine Nielsen's combined diffusion

Table 3. Average Percent Difference Between Observed and Modeled Concentration at 30 cm Above the Bed During the Storm and Swell Conditions [100abs($C_m - C_{obs}$)/mean(C_m, C_{obs})][a]

Model	Advection, ϵ_m	Storm		Swell	
		Mean	Confidence Interval (95%)	Mean	Confidence Interval (95%)
GMG single	no, two layer	28.19	3.47	49.66	0.50
GMG	no, two layer	16.22	3.02	43.80	2.20
GMG no armor	no, two layer	49.12	0.30	49.22	0.23
Nielsen	no, constant	46.39	0.74	47.08	1.07
Nielsen	yes, constant	33.44	1.59	38.18	3.60
GMGW	no, three layer	14.53	3.16	45.15	1.65
GMGW	yes, three layer	18.26	3.00	46.22	1.41
GMG thick	no, two layer	16.22	3.02	16.07	3.10

[a] All models include multiple grain sizes and bed armoring except for GMG single and GMG no armor. Only GMG thick includes a thickened WBL when $R > 1.0$.

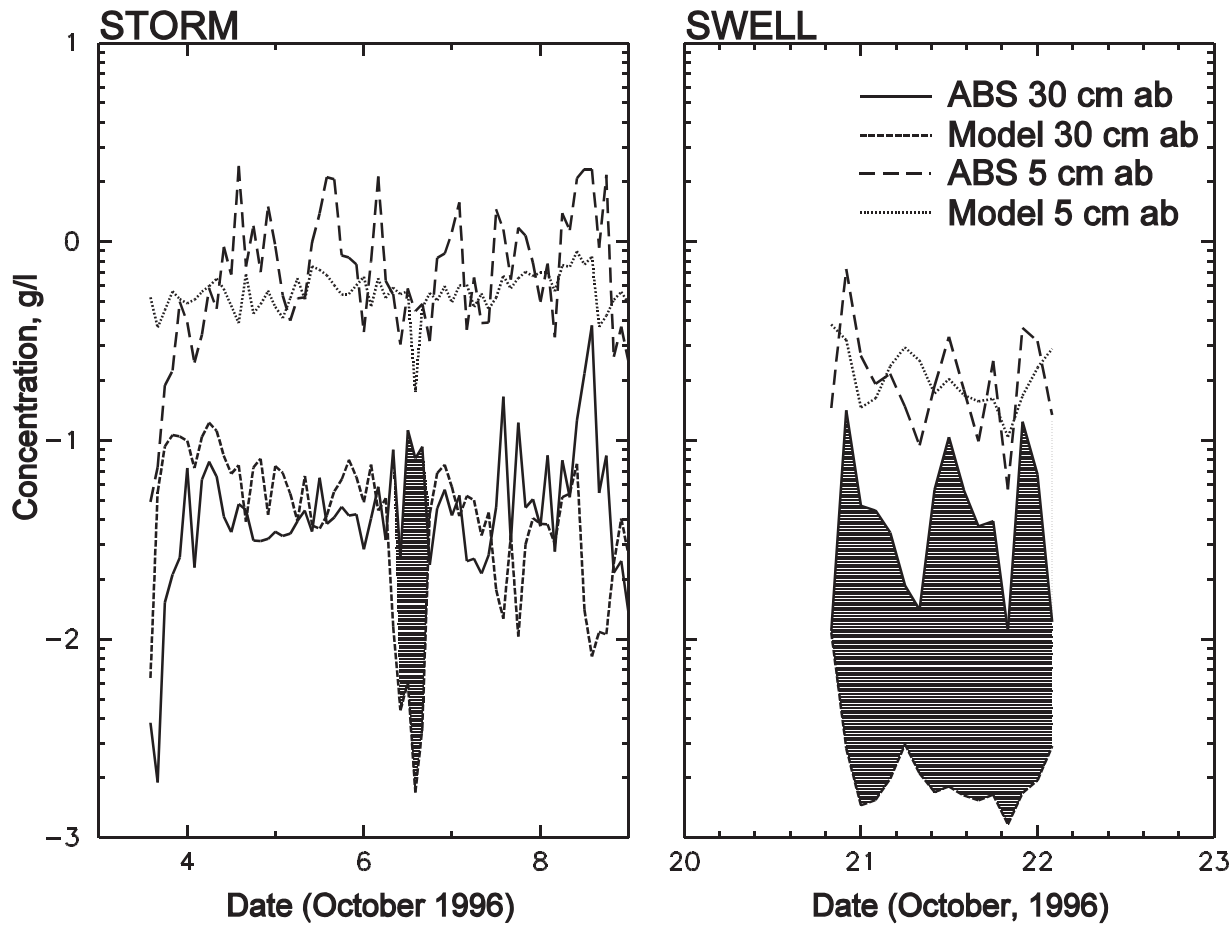

Figure 14. Time series of observed and GMG model concentration at 5 and 30 cm ab during (left) storm and (right) swell conditions. Shading indicates times when the assumption of equation (4) is likely invalid.

and advection model using a linearly increasing eddy diffusivity. Nielsen's approach requires viscosity to be continuous. Otherwise, the concentration profile is not continuous at the top of the WBL. Since the two-layered eddy viscosity model is discontinuous, the modified three-layered eddy viscosity model of *Madsen and Wikramanayake* [1991] (GMGW model) is adopted. The profile of eddy diffusivity is expressed by the following equation:

$$\epsilon_m = \epsilon_s = \kappa u_{*_{cw}} z, \qquad 0 \le z \le \delta_w, \tag{24a}$$

$$\kappa u_{*_{cw}} \delta_w, \qquad \delta_w \le z \le \delta_w/\delta_\alpha, \tag{24b}$$

$$\kappa u_{*_c} z, \qquad \delta_w/\delta_\alpha \le z. \tag{24c}$$

The intermediate layer, $\delta_w \le z \le \delta_w/\delta_a$, allows a transition from the wave boundary layer to the current boundary layer. The height of this layer is scaled by $\delta_\alpha = u_{*c}/u_{*cw}$. Adopting the three-layered eddy diffusivity model, the solutions for equation (7) using equation (24) and $P = w_s C_{ri}$ are provided by *Lee and Hanes* [1996]. The parameters used in this model were obtained from the GMGW model and bed armoring effects with seven grain sizes were incorporated as in the other models. Figure 16 also shows concentration profiles predicted by GMGW plus advection during storm and swell. Table 3 indicates that above the wave boundary layer, adding advection as formulated by *Lee and Hanes* [1996] actually made the GMGW model do worse overall during both storm and swell.

7. Discussion and Conclusions

[37] Observations of sediment concentration exhibited two distinctive patterns: high near-bed concentration that decreased rapidly with height above the bed during the storm versus lower near-bed concentration which decreased much more slowly with height during swell. Perturbations in near-bed concentration associated with bed form crests also dissipated more rapidly with elevation during the storm relative to swell. Our analysis was focused on evaluating the significance of the various mixing processes that possibly produce the observed patterns and the conditions under which each process dominates. Two dominant mixing processes, diffusion and advection, were evaluated by examining sediment suspension models. In addition, the assumption of equality between eddy viscosity and eddy diffusivity was examined.

[43] Eddy diffusivity was inferred from the observed concentrations. Our results showed that there was a near-

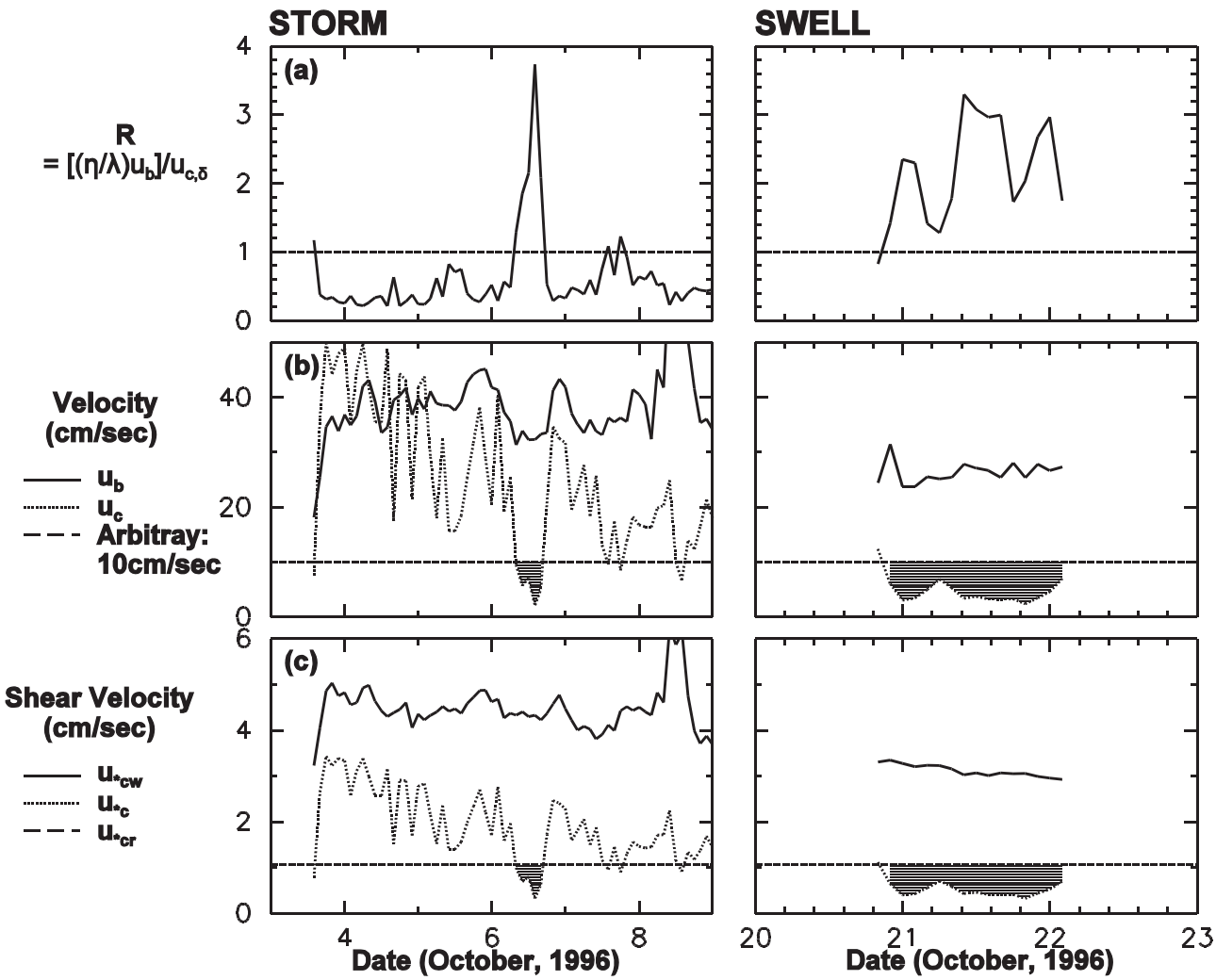

Figure 15. (a) Time series of scaling parameter, R, which is a ratio of the vertical advection velocity to the mean current, $u_{c,\delta}$ at the top of the wave boundary layer during (left) storm and (right) swell conditions. The vertical advection velocity u_j is scaled to $(\eta/\lambda)u_b$, where η and λ are the ripple height and ripple length, respectively, and u_b is the maximum near-bottom orbital velocity; (b) current velocity and near-bottom wave orbital velocity. Arbitrary line is set to delineate weak current condition; (c) Time series of shear velocities of $u_{*c,\mathrm{model}}$, u_{*cw}, and u_{*cr} for the mean sediment size.

bottom region over which eddy diffusivity increases linearly during both storm and swell conditions (Figure 10). Assuming a diffusive balance, shear velocity inferred from the linearly increasing eddy diffusivity profiles ($u_*\epsilon_s$) agreed well with shear velocity owing to the mean current (u_{*cw}) during the storm and shear velocity due to waves plus current (u_{*cw}) during swell (Figure 10). The conditions for which eddy diffusivity above the classical wave boundary layer were associated with u_{*c} or u_{*cw} were delineated by the scaling parameter, R, which is the ratio of jet velocity associated with vortex shedding off bed roughness elements relative to the crossflow velocity associated with the mean current. The period that $u_{*\varepsilon s}$ agreed with u_{*c} corresponded to the period of low R values ($R < 1.0$) and strong currents. Higher R values ($R > 1.0$) and weak currents corresponded to the period of $u_{*\varepsilon s} = u_{*cw}$. It is suggested that strong current (low R) block vortices shed by waves over ripples from extending beyond the predicted WBL. In the absence of a strong mean current (high R), sediment-laden vortices are injected well above the classical WBL, reducing the decay of the mean concentration profile with height above the bed.

[39] Six sediment suspension models were examined: the two-layered GMG Rouse-type model with and without multiple grain sizes/bed-armoring, Nielsen's constant eddy diffusivity model with and without vertical advection, and the three-layered GMGW model also with and without vertical advection, with the latter four all including multiple grain sizes and armoring. During strong current conditions when turbulent diffusion associated with the mean current is a dominant process, the GMG/W models without advection reproduced the observed concentration well. In all cases, bed armoring with graded sediment sizes was important in order to produce reasonable concentrations. The constant eddy diffusivity models underpredictd concentration during the storm because the

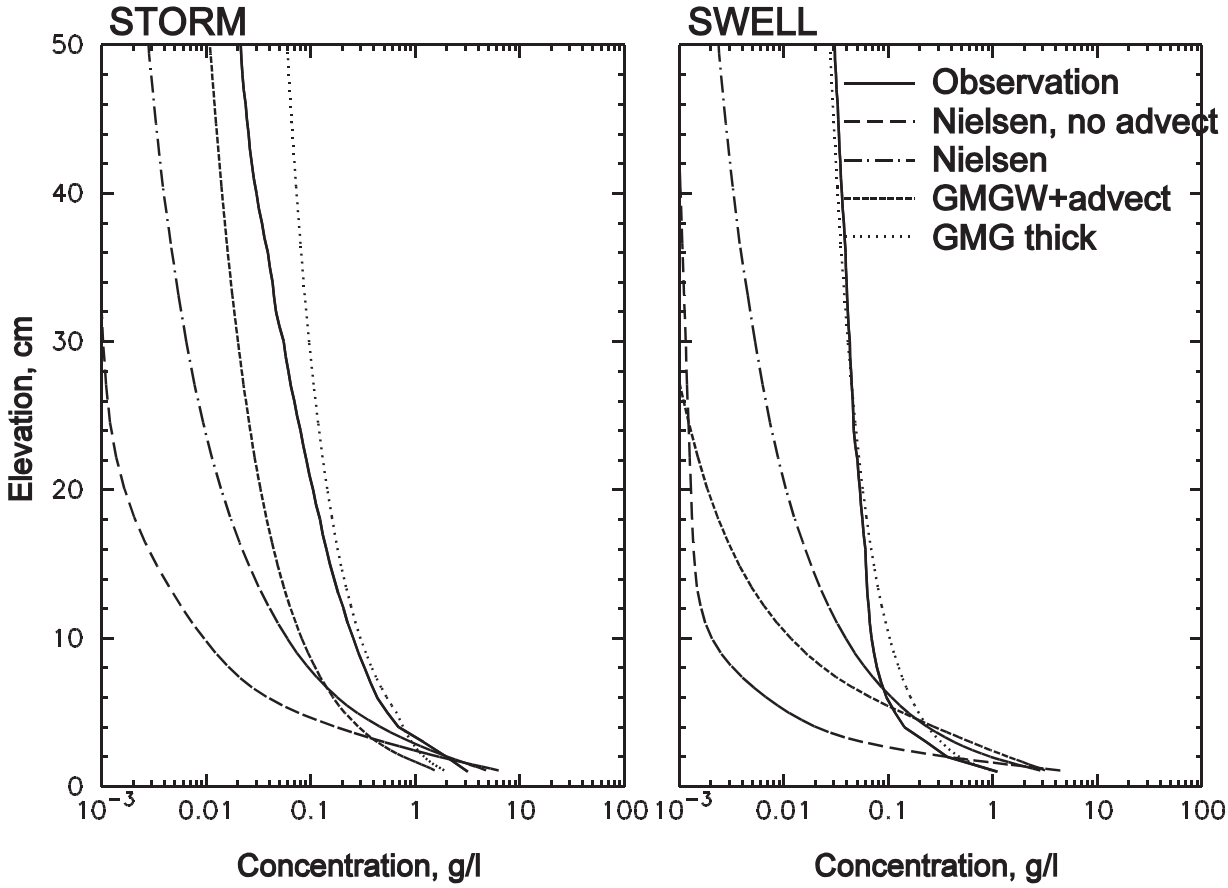

Figure 16. Sediment concentration profiles during (left) storm and (right) swell. Combined diffusion and advection model of *Nielsen* [1992] is compared with the observed concentration, the Nielsen model with no advection, the three-layer GMGW model with advection, and the two-layered GMG model with a thickened wave boundary layer of $R > 1.0$.

constant eddy diffusivity of O(1 cm^2/s) was inadequate more than a few centimeters into the water column. During weak currents in the presence of strong waves all the models underpredicted the observed concentrations. Note that it has been argued in the literature that the vertical distribution of suspended sediment under waves is best described by equation (3) using a constant eddy diffusivity, which results in an exponential concentration profile [e.g., *Nielsen*, 1992]. However, our swell data suggest that eddy diffusivity above ripples under waves may be a strong function of height above the bed and that the mean concentration profile may not be exponential. This may be due to the fact that the predicted ripple height (1–2 cm) and steepness (0.12) in our case were relatively low. For larger, steeper ripples with vigorous vortex shedding, Nielsen's argument could still be valid.

[40] Observations and modeling both reinforce the conclusion that turbulent diffusion associated with current shear above the wave boundary layer is the dominant process for sediment suspension during strong current conditions. An interesting finding is that eddy diffusivity associated with u_{*cw} may extend well above the predicted wave boundary layer during weak current conditions. One possible explanation is that turbulent-like mixing above the classical wave boundary layer under weak currents is driven by the fluid advected up from the wave boundary layer. For example, *Sleath* [1990] reasoned that even though vortex shedding is clearly different from turbulence, shedding of vortices produces a vertical exchange that has a net effect similar to that of turbulence. If organized vortex shedding has turbulent properties when averaged at large enough scale, then it is possible that an effective eddy viscosity can still be usefully applied to model both mass and momentum exchange by ripple induced vortices. In some respect, application of an "effective" eddy viscosity equal to eddy diffusivity is physically more attractive than adding a term for advection of mass alone because the latter neglects the associated transfer of momentum.

[41] Figure 16 shows the observed and predicted concentrations of the two-layered Rouse model (equation (19)) during swell conditions using an effective diffusivity associated with u_{*cw} up to a height of 50 cm. The agreement between them is quite good (see also Table 3). Admittedly, the observations during swell do not support $u_* = u_{*cw}$ all the way to 50 cm; however, they do support a value for u_* much larger than that predicted by GMG at that height (see Figure 10). A goal of this analysis is to suggest as simple a model as possible, and setting $u_* = u_{*cw}$ throughout the observed

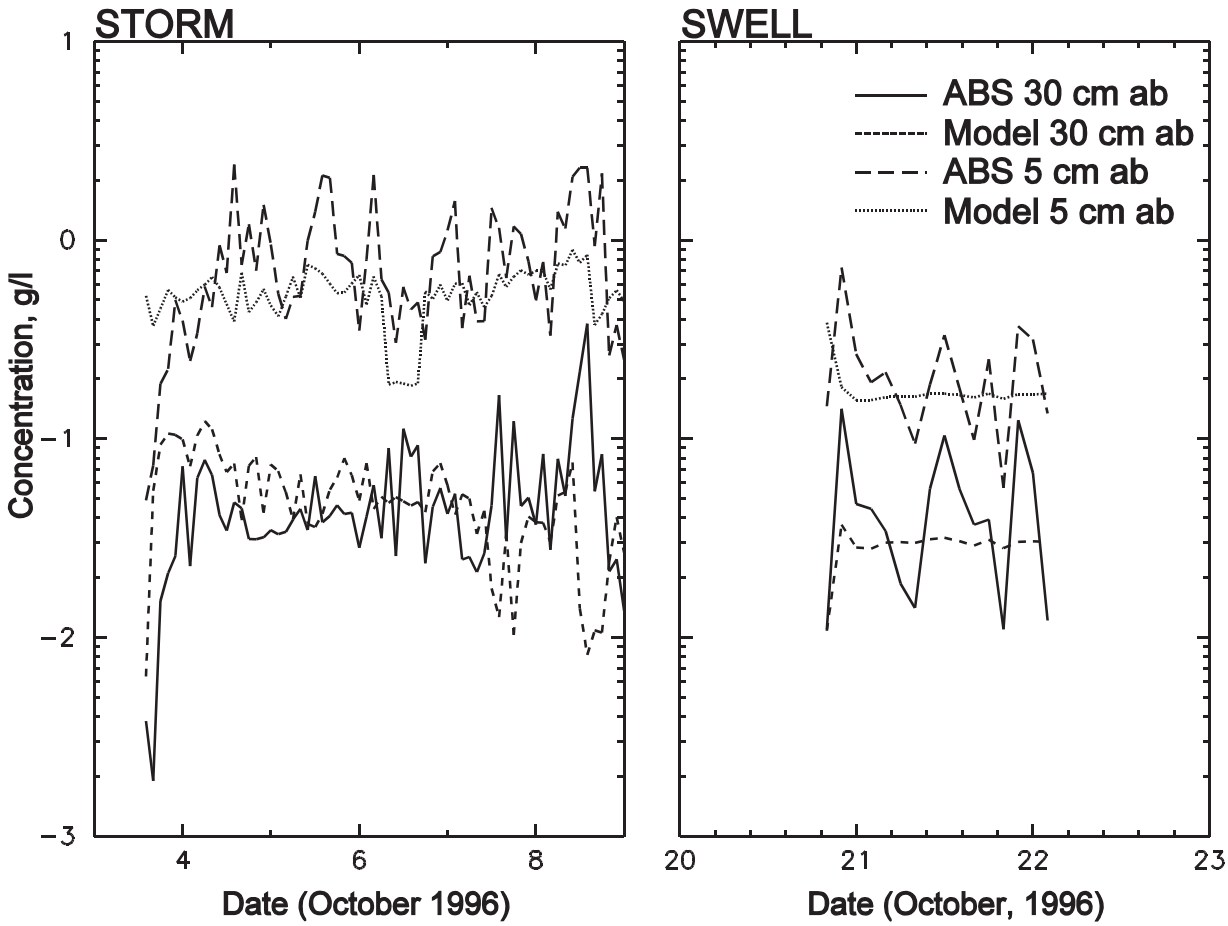

Figure 17. Time series of observed and GMG-thick model concentraton at 5 and 30 cm ab during (left) storm and (right) swell conditions. GMG-thick is equivalent to GMG except that when $R > 1.0$, u_{*cw} is used to formulate eddy diffusivity up to 50 cm ab.

concentration profile for $R > 1.0$ is particularly straightforward. Figure 17 shows the time-series of observed and predicted concentrations during storm and swell with the effective WBL thickness set to 50 cm for cases with $R > 1.0$. The plot shows the improved prediction at 30 cm ab during the weak current conditions (compare the plot to Figure 14). Table 4 briefly summarizes the step-by-step methodology used to produce this final model. During swell conditions the predictions in Figure 17 still do not mimic the observed higher (and lower) concentrations above the ripple crest (and trough) but result in somewhat average concentrations over the period of swell as a whole. This indicates that the estimation of shear stresses by the wave and current interaction model and the concentrations predicted by the Rouse equation are spatial averages of heterogeneous areal features.

[42] It is important to consider also how sensitive the predicted current profile is to changes in the effective viscosity profile. Figure 18 shows observed and modeled current velocities during the storm and swell for the lower two current meters (initially 19 and 38 cm ab). Three wave boundary layer thicknesses were used in the velocity model: (1) the GMG prediction, δ_w, (2) twice δ_w, and (3) the maximum height of the linearly increasing eddy diffusivity inferred from the concentration profiles, $\delta_{\epsilon s}$. Velocities in Figure 18 were predicted by starting with observed velocity from a higher current meter (at 98 cm ab) and then applying current shear according to u_{*c}, u_{*cw}, and the chosen WBL thickness. The error estimates at lower sensor heights between the observed velocity and the predicted velocities for the three wave boundary layer thicknesses ranged from 38 to 39%. However, the disagreement among the predicted velocities were under 2%. Thus the resolution of current shear provided by the current meters was too low to distinguish between the various choices of WBL thickness. In other words, thickening the effective WBL during periods of low current made relatively little difference to the current profile and was no more inconsistent with the observed currents than application of a thinner WBL.

[43] Most boundary layer wave and current interaction models do not consider the effect of shedding vortices and the resulting enhanced vertical exchange above the wave boundary. Those that do so via an advection term do not adequately reproduce the relative slow decay of concentration with height above the bed observed under weak current conditions [*Lee and Hanes*, 1996; this paper]. This effect still needs to be incorporated into wave and current interaction models in order to better describe vertical mixing and to predict sediment concen-

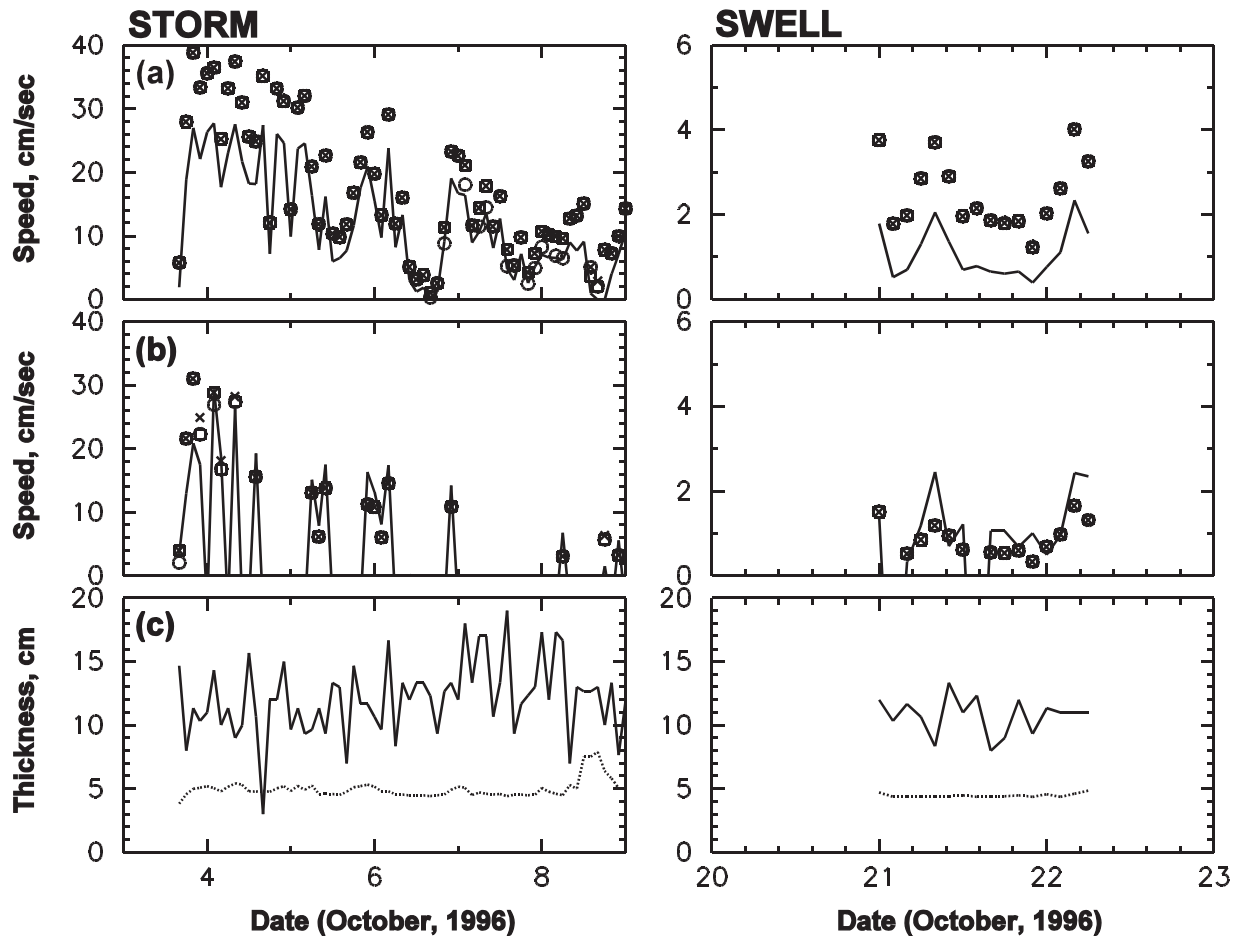

Figure 18. Time series of observed (solid line) and predicted burst-averaged current velocities for the storm and swell periods: (a) electromagnetic current meters initially at 38 cm ab, (b) acoustic Doppler velocimeter (ADV) initially at 19 cm ab. Predictions with break in eddy viscosity at δ_w (cross), $2\delta_w$ (square), and $\delta_{\epsilon w}$ (circle). Observed data are not shown for bursts when the ADV was too close to the bed to accurately record velocity. (c) GMG prediction of wave boundary layer thickness (δ_w, dotted line) and observed top of linearly increasing eddy diffusivity ($\delta_{\epsilon w}$, solid line).

tration more accurately. Perhaps one viable approach is use of an effective diffusivity that parameterizes this enhanced exchange as being similar to turbulence when averaged horizontally and temporally. Further field observations of flow structure in this region are required to examine the validity of this hypothesis, particularly with respect to its effect on mean current shear very close to the bed.

Table 4. Steps in Final Application of GMG Model With Thickened Wave Boundary Layer

Step	Methodology
1	Inputs: burst-averaged current at one height, rms wave orbital velocity, wave period, wave-current angle, distribution of seven size classes in the bed
2	Apply Wiberg-Harris ripple model.
3	Apply two-layered Grant-Madsen model to determine u_{*c}, u_{*cw}, and δ_w. It is necessary to iterate with the Xu-Wright relation for moveable bed roughness.
4	Apply the two-layered Glenn-Grant model for suspended sediment distribution. It is necessary to iterate with the Wiberg bed armoring model.
5	Apply a WBL thickness of 50 cm to the suspension model if $R > 1.0$; apply the standard δ_w otherwise.

[44] **Acknowledgments.** This study was supported by National Science Foundation grants OCE-9504198 and OCE-9633182. We thank the Virginia Institute of Marine Science (VIMS) Physical Sciences Department technical staff for their tireless efforts in constructing, calibrating, programming, deploying, and retrieving the tripod instrumentation. The anonymous reviewers of this manuscript provided extremely useful comments. This is contribution number 2407 from the Virginia Institute of Marine Science.

References

Amos, C. L., A. J. Bowen, D. A. Huntley, and C. F. M. Lewis, Ripple generation under the combined influences of waves and currents on the Canadian continental shelf, *Cont. Shelf Res.*, *8*, 1129–1153, 1998.

Andreapoulos, J., and W. Rodi, Experimental investigation of jets in a crossflow, *J. Fluid Mech.*, *138*, 93–127, 1984.

Birkemeier, W. A., H. C. Miller, S. D. Wilhelm, A. E. DeWall, and C. S. Gorbics, A user's guide to the Coastal Engineering Research Center's Field Research Facility, *Instruct. Rep. CERC-85-1*, Coastal Eng. Res. Cent., U.S. Army Corps of Eng., Vicksburg, Miss., 1985.

Dick, J. E., and J. F. A. Sleath, Velocities and concentrations in oscillatory flow over beds of sediment, *J. Fluid Mech.*, *233*, 165–196, 1991.

Dietrichs, W. E., Settling velocity of natural particles, *Water Resour. Res.*, *18*, 1615–1626, 1982.

Dyer, K. R., *Coastal and Estuarine Sediment Dynamics*, 342 pp., John Wiley, New York, 1986.
Folk, R. L., *Petrology of Sedimentary Rock*, 182 pp., Hemphill, Austin, Tex., 1968.
Glenn, S. M., and W. D. Grant, A suspended sediment stratification correction for combined wave and current flow, *J. Geophys. Res.*, *92*, 8244–8264, 1987.
Grant, W. D., and O. S. Madsen, The continental shelf bottom boundary layer, *Annu. Rev. Fluid Mech.*, *18*, 265–305, 1986.
Lee, T. H., and D. M. Hanes, Comparison of field observations of the vertical distribution of suspended sand and its prediction by models, *J. Geophys. Res.*, *101*, 3561–3572, 1996.
Leffler, M. W., C. F. Baron, B. L. Scarborough, K. K. Hathaway, and R. T. Hayes, Annual data summary for 1991, CERC Field Research Facility, vol. 1, Main Text and Appendix A and B, *Technical Rep. CERC-93-3*, Coastal Eng. Res. Cent., U.S. Army Corps of Eng., Vicksburg, Miss., 1993.
Li, M. Z., C. L. Amos, and D. E. Heffler, Boundary layer dynamics and sediment transport under storm and non-storm conditions on the Scotian Shelf, *Mar. Geol.*, *141*, 157–181, 1997.
Lynch, J. F., J. D. Irish, T. F. Gross, P. L. Wiberg, A. E. Newhall, P. A. Traykovski, and J. D. Warren, Acoustic measurements of the spatial and temporal structure of the near-bottom boundary layer in the 1990–1991 STRESS experiment, *Cont. Shelf Res.*, *17*, 1271–1295, 1997.
Madsen, O. S., and P. L. Wikramanayake, Simple models for turbulent wave-current bottom boundary layer flow, *Contract Rep. DRP-91–1*, Coastal Eng. Res. Cent., U.S. Army Corps of Eng., Vicksburg, Miss., 1991.
Madsen, O. S., L. D. Wright, J. D. Boon, and T. A. Chisholm, Wind stress, bed roughness and sediment suspension on inner shelf during an extreme storm event, *Cont. Shelf Res.*, *13*, 1303–1324, 1993.
Meyer-Peter, E., and R. Müller, Formulas for bedload transport, in *Proceedings of the Second Meeting*, pp. 39–64, Int. Assoc. of Hydraul. Res, Stockholm, Sweden., 1948.
Nielsen, P., Field measurements of time-averaged suspended sediment concentrations under waves, *Coastal Eng.*, *8*, 51–72, 1984.
Nielsen, P., *Coastal Bottom Boundary Layers and Sediment Transport*, 324 pp., World Sci., River Edge, N. J., 1992.
Osborne, P. D., and C. E. Vincent, Vertical and horizontal structure in suspended sand concnetrations and wave-induced fluxes over bedforms, *Mar. Geol.*, *131*, 195–208, 1996.
Ribberink, J. S., and A. A. Al-Salem, Sediment transport in oscillatory boundary layers in cases of rippled beds and sheet flow, *J. Geophys. Res.*, *99*, 12,707–12,727, 1994.
Sheng, J., and A. E. Hay, Sediment eddy diffusivities in the nearshore zone, from multifrequency acoustic backscatter, *Cont. Shelf Res.*, *15*, 129–147, 1995.
Sleath, J. F. A., The suspension of sand by waves, *J. Hydraul. Res.*, *20*, 439–452, 1982.
Sleath, J. F. A., *Sea Bed Mechanics*, 355 pp., John Wiley, New York, 1984.
Sleath, J. F. A., Seabed boundary layers, in *The Sea*, vol. 9B, edited by B. Le Méhauté, and D. M. Hanes, pp. 693–728, John Wiley, New York, 1990.
Smith, J. D., Modeling of sediment transport on continental shelves, in *The Sea*, vol. 6, edited by E. D. Goldberg et al., pp. 539–577, John Wiley, New York, 1977.
Thorne, P. D., P. J. Hardcastle, and R. L. Soulsby, Analysis of acoustic measurements of suspended sediments, *J. Geophys. Res.*, *98*, 899–910, 1993.
Van Rijn, L. C., W. C. Nieuwjaar, T. Van Der Kaay, E. Nap, and A. Van Kampen, Transport of fine sands by currents and waves, *J. Waterw. Port Coastal Ocean Eng.*, *119*, 123–143, 1993.
Vanoni, V. A., *Sedimentation Engineering*, 745 pp., Am. Soc. of Civ. Eng., Reston, Va., 1975.
Vincent, C. E., and A. Downing, Variability of suspended sand concentrations, transport and eddy diffusivity under non-breaking waves on the shoreface, *Cont. Shelf Res.*, *14*, 223–250, 1994.
Vincent, C. E., and M. O. Green, Field measurements of the suspended sand concentration profiles and fluxes and of the resuspension coefficient γ_o over a rippled bed, *J. Geophys. Res.*, *95*, 11,591–11,601, 1990.
Vincent, C. E., and P. D. Osborne, Predicting suspended sand concentration profiles on a macro-tidal beach, *Cont. Shelf Res.*, *15*, 1497–1514, 1995.
Wai, O. W. H., K. W. Bedford, C. M. Libicki, and R. E. Van Evra, The structural evolution of a wave current sediment concentration boundary layer, in *Coastal Sediment'91*, pp. 342–355, Am. Soc. of Civ. Eng., Reston, Va., 1991.
Wiberg, P. L., and C. K. Harris, Ripple geometry in wave-dominated environments, *J. Geophys. Res.*, *99*, 775–789, 1994.
Wiberg, P. L., D. E. Drake, and D. A. Cacchione, Sediment suspension and bed armoring during high bottom stress events on the northern California inner continental shelf: measurements and predictions, *Cont. Shelf Res.*, *14*, 1191–1219, 1994.
Xu, J. P., and L. D. Wright, Tests of bed roughness models using field data from the Middle Atlantic Bight, *Cont. Shelf Res.*, *15*, 1409–1434, 1995.

C. T. Friedrichs, Virginia Institute of Marine Science, School of Marine Science, College of William and Mary, Gloucester Point, VA 23062, USA.
G.-H. Lee, Institute of Theoretical Geophysics, University of Cambridge, Downing Street, Cambridge, CB2 3EQ, UK. (glee@esc.cam.ac.uk)
C. E. Vincent, School of Environmental Science, University of East Anglia, Norwich, NR4 6TJ, UK.

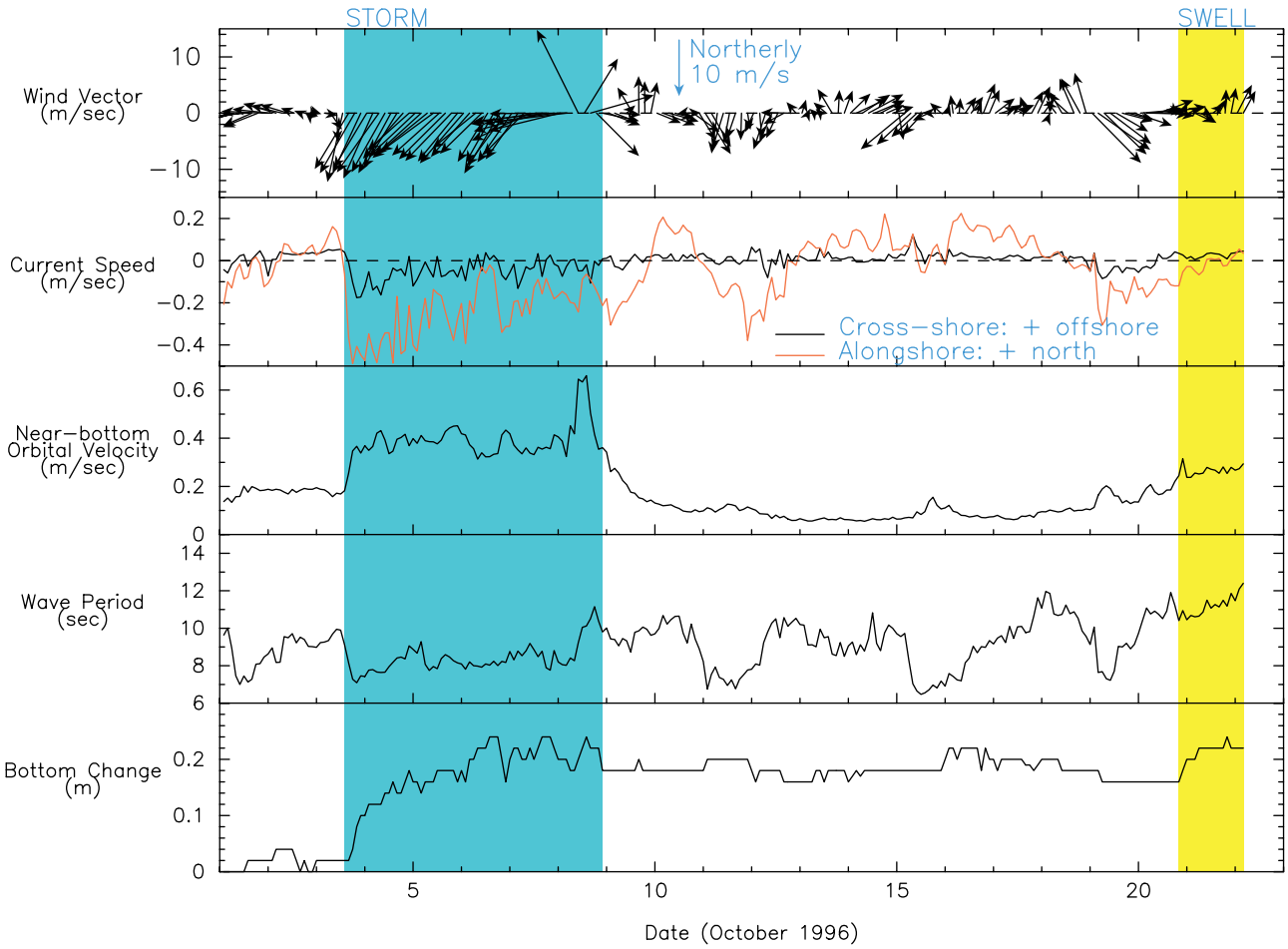

Figure 4. Environmental conditions during VIMS tripod deployment. Storm and swell conditions are delineated by vertical lines.

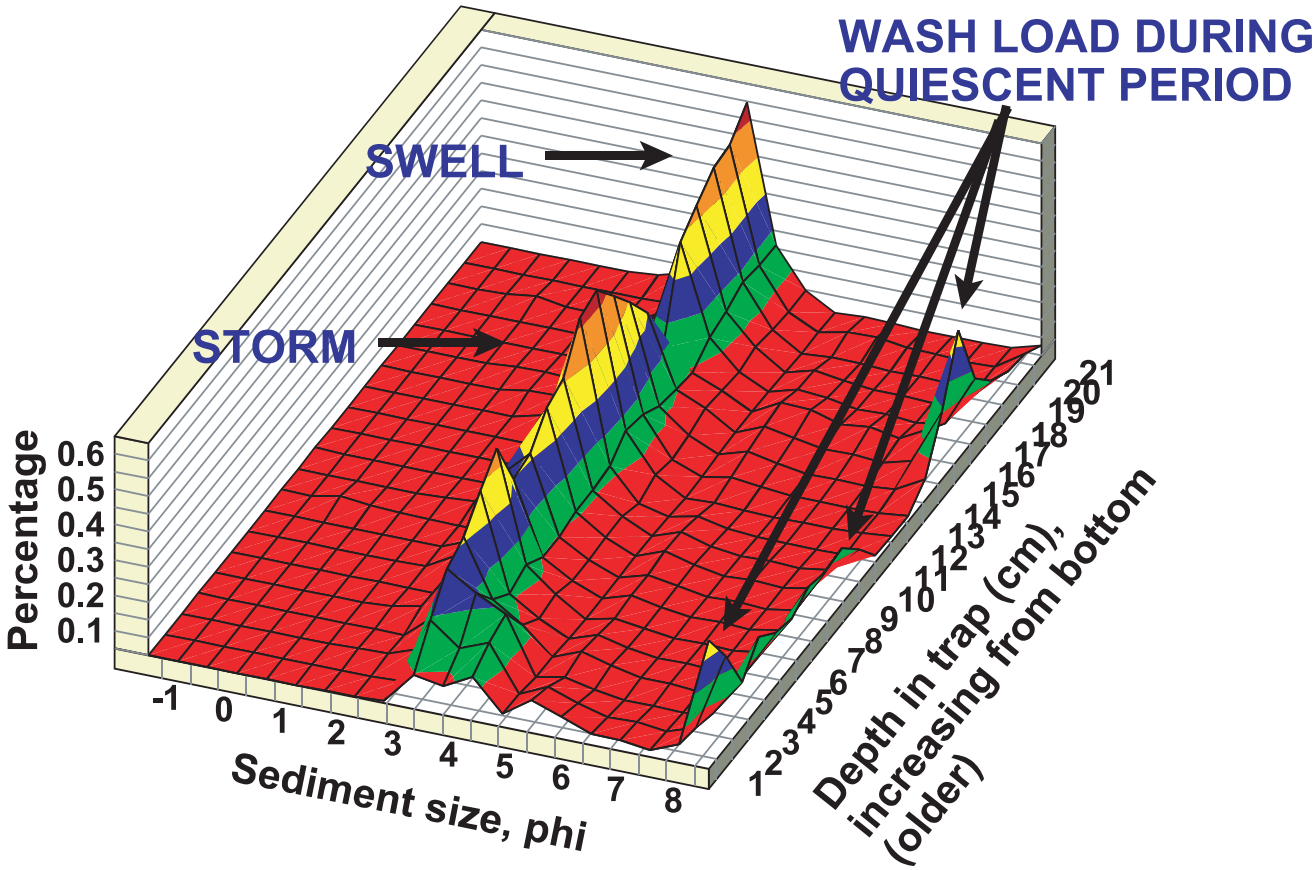

Figure 5. Sediment size fractions of trap sediment. A significant increase in percent fine sediment deposition is seen between coarser storm and swell deposits.

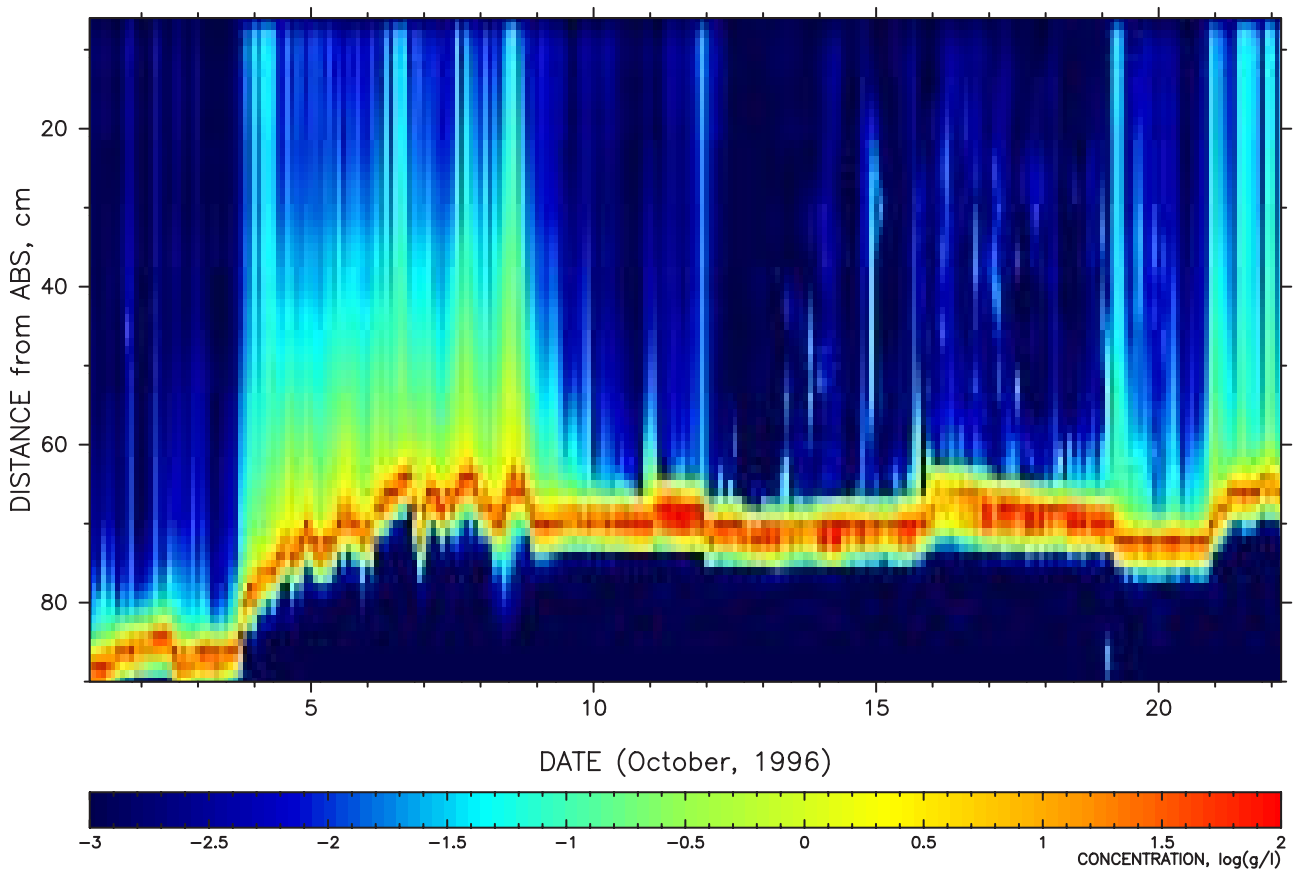

Figure 6. Burst-averaged sediment concentration during the deployment. Relatively high sediment suspension occured during the storm (4–8 October, 1996) and swell (20–21 October), but virtually no suspension occured during the fairweather condition (10–20 October). Bed elevation relative to the sensors increased by ∼20 cm during the storm.

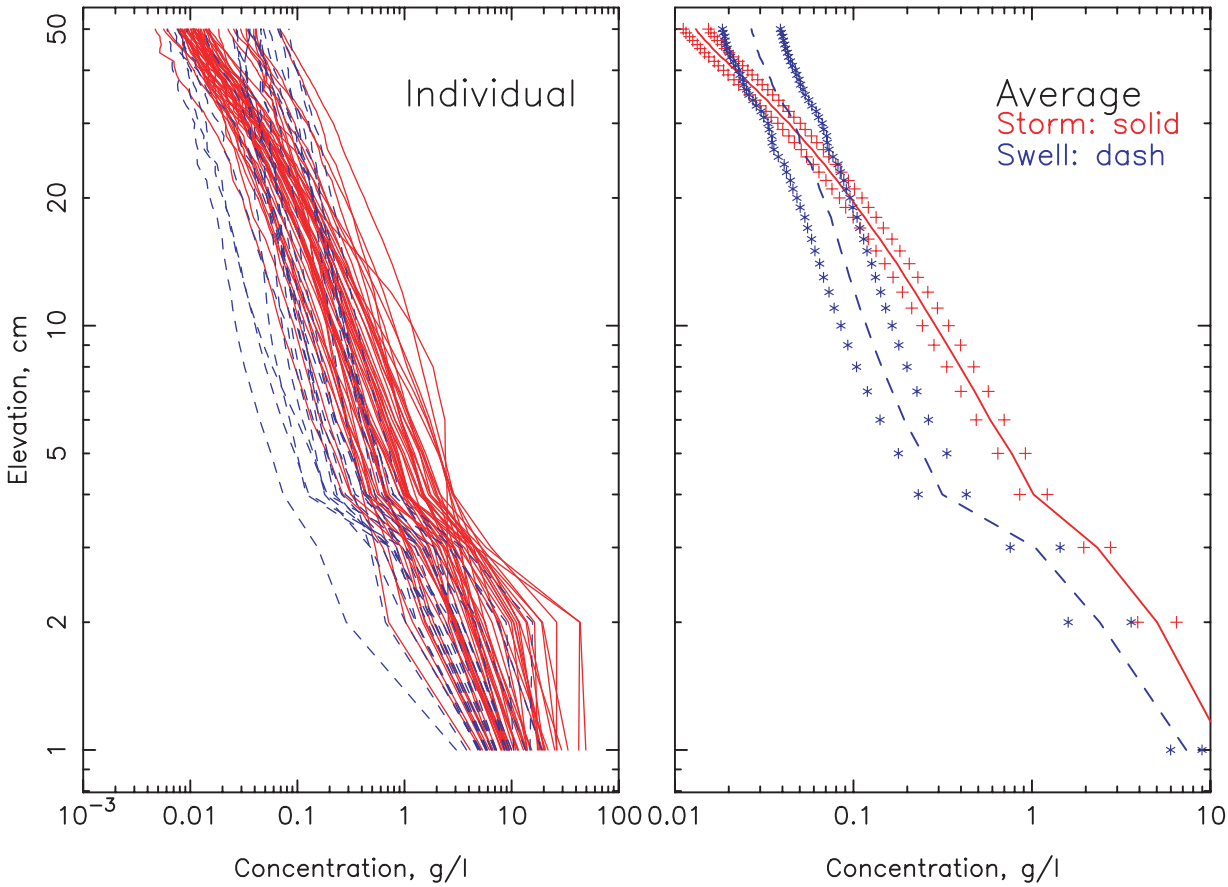

Figure 7. Average sediment concentration profile during the storm and swell. Plus and asterisks indicate 95% confidence interval of storm and swell average sediment concentration profiles, respectively. Near-bottom sediment concentration during the storm was higher (by a factor of 2) than during the swell. However, the concentration gradient (decay rate) with elevation was greater during the storm.

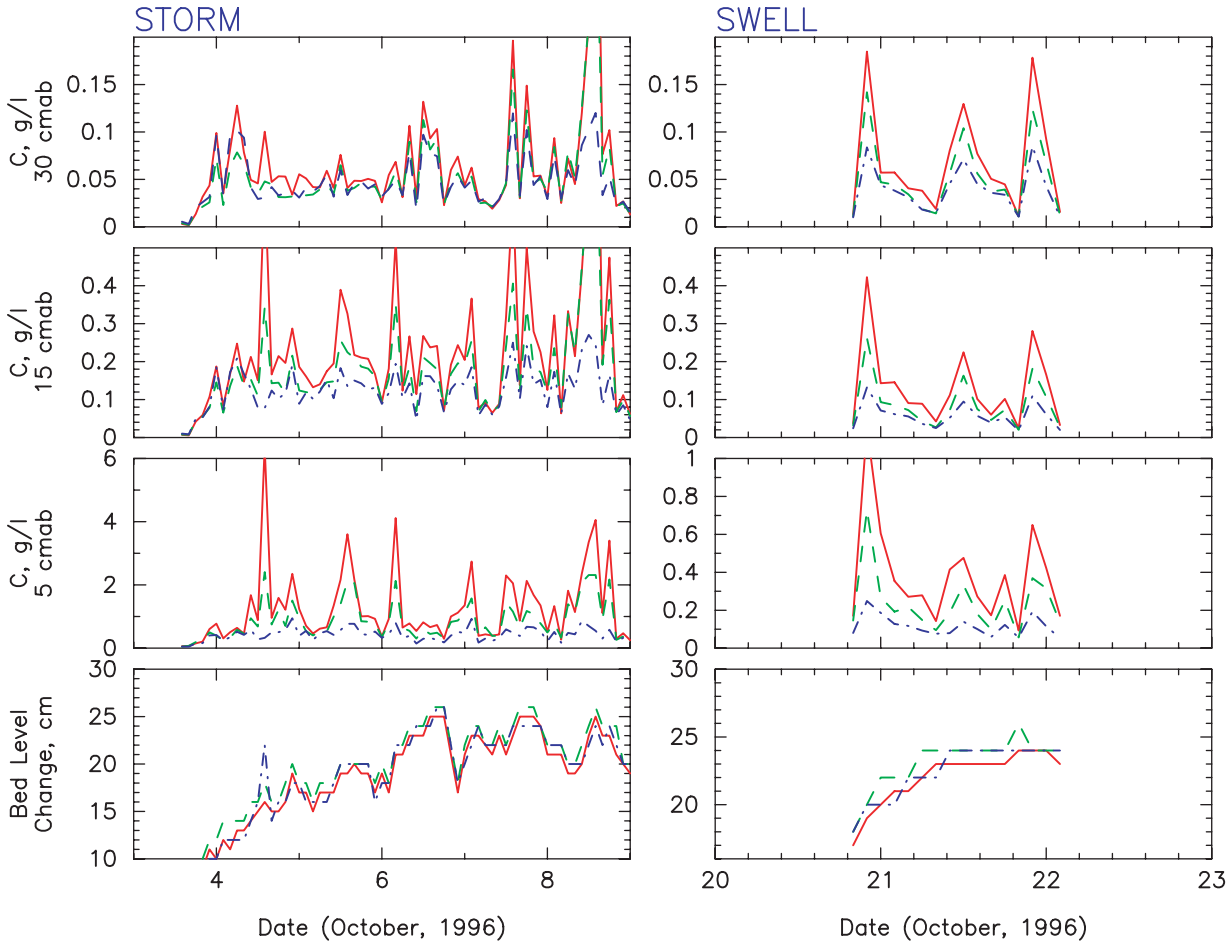

Figure 8. Observed sediment concentration at 5, 15, and 30 cm ab and observed bed level change during (left) storm and (right) swell. Higher resuspension above bedform crests is inferred for both storm and swell. A vertically coherent pattern of higher concentration above bedforms continues up to ~20 cm during storm and above 30 cm during swell. Above 20 cm ab during the storm, higher concentration does not necessarily correspond to bedform location, suggesting a different vertical mixing mechanism is at work. Solid line, F1; dash, F2; dot, F3.

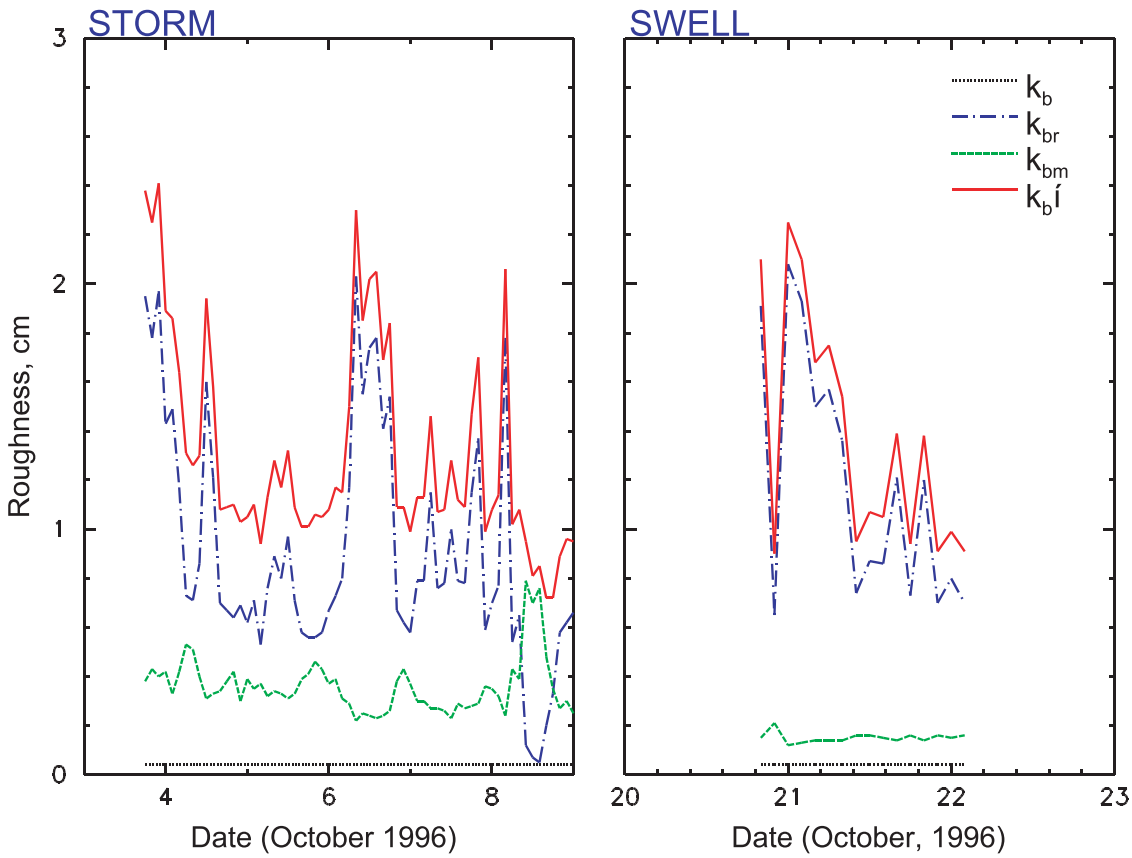

Figure 9. Modeled bed roughness during (left) storm and (right) swell. The k_b value is grain roughness, k_{br} is drag roughness due to ripples, k_{bm} is movable bed roughness, and k_b' is total roughness.

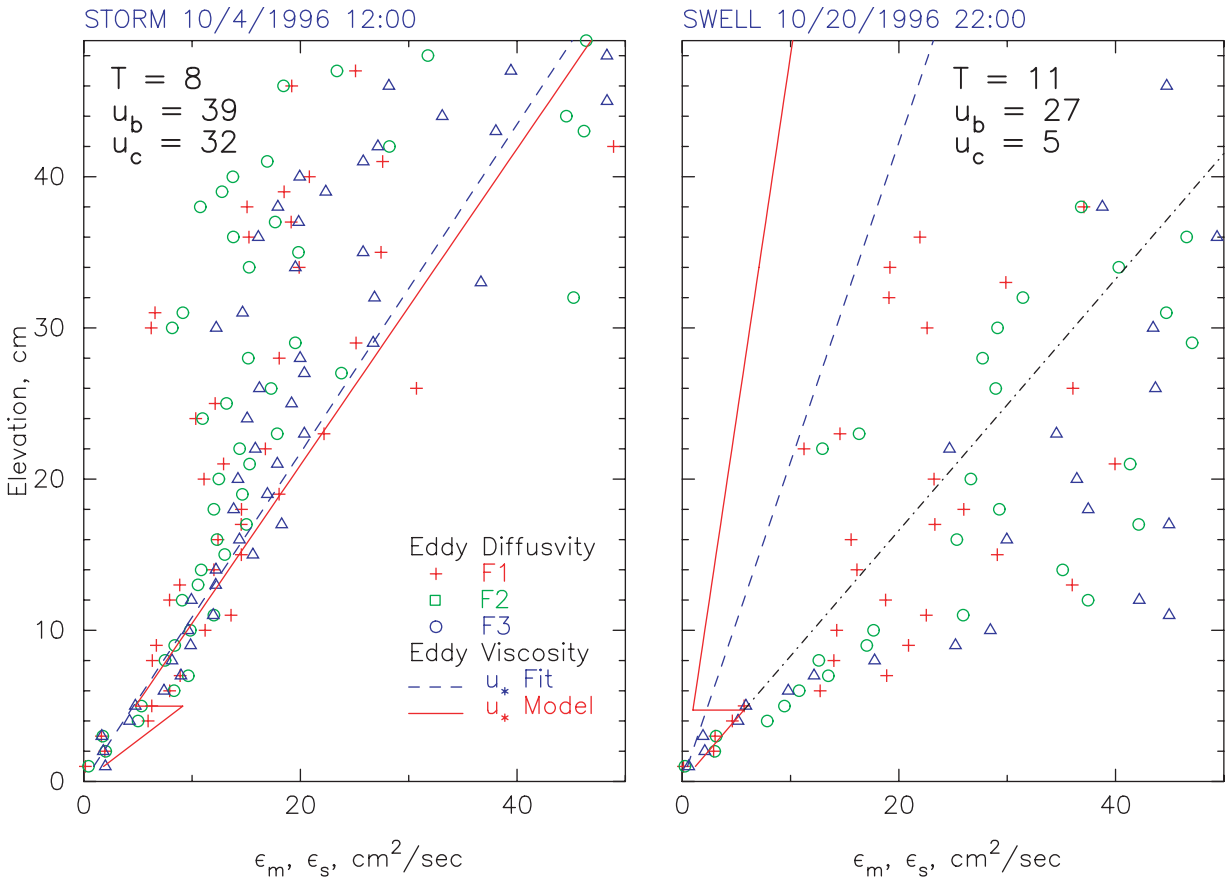

Figure 10. Eddy viscosity and diffusivity profiles during (left) storm conditions on 5 October 1996 at 0800 UT and (right) swell conditions on 22 October 1996 at 0000 UT. The $u_{*\mathrm{fit}}$ is from the observed current profile, and $u_{*\mathrm{model}}$ is predicted by the Grant-Madsen-Glenn (GMG) model. Eddy viscosity using u_{*cw} above the wave boundary layer is shown by a dotted line for the swell case. Wave period T, current speed at 1 m ab u_c, and near-bottom orbital velocity u_b are also shown.